Earthquake-induced landslides susceptibility evaluation: a case study from the Abruzzo Region (Central Italy)

Cristiano Carabella[1], Jacopo Cinosi[1], Valerio Piattelli[1], Pierfrancesco Burrato[2], Enrico Miccadei[1,2,*]

Affiliations:

[1]Department of Engineering and Geology, Università degli Studi "G. d'Annunzio" of Chieti-Pescara, Via dei Vestini 31, 66100 Chieti, Italy.

[2] Istituto Nazionale di Geofisica e Vulcanologia, Sezione Roma 1, Via di Vigna Murata 605, 00143 Rome, Italy.

Corresponding author: enrico.miccadei@unich.it (E.M.)

Authors' emails: cristiano.carabella@unich.it (C.C.), jacopocinosi@yahoo.it (J.C.), valerio_piattelli@msn.com (V.P.), pierfrancesco.burrato@ingv.it (P.B.)

Abstract

Landslides are widespread natural phenomena that play an important role in landscape evolution and are responsible for several casualties and damages. Slope instability is linked to the combination of geological, geomorphological, and climatic factors with various triggering mechanisms; among these, seismic shaking can induce relevant changes in the landscape, leading to coseismic and post-seismic phenomena such as landslide events. The Abruzzo Region (Central Italy) is severely affected by Earthquake-Induced Landslides (EILs), linked to the geomorphological dynamics and the severe seismicity of the area. The distribution, mechanisms, and typology of landslides are strictly related to the different physiographic and geological-structural settings. This paper focuses on the realisation of an EILs susceptibility map, following a heuristic approach combined with a statistical analysis, integrated using GIS technology. This approach led to the identification of nine instability factors.

These factors were analysed for the construction of thematic maps. Hence, each factor was assigned proper expert-based ranks and weights based on the critical evaluation of literature data as well as on available landslide inventories and combined in a preliminary map wherein high/low numerical values correspond to a high/low propensity of the slope to fail; furthermore, a statistical analysis of these values was performed to derive suitable susceptibility classes. Results presented herein highlight the robustness of the approach; remarkably, the applied methodology is suitable even in areas where a detailed landslide catalogue is lacking, when the same classification and weighting of available parameters is performed. The statistical analyses and the adoption of an absolute scale ranging from minimum to maximum potential values, finally, ensures the comparability of results among different study areas. Finally, this work represents a scientific and multidisciplinary tool for better defining situations that could lead to hazards (such as landslides) following an earthquake to develop sustainable territorial planning, emergency management, and loss-reduction measures.

Keywords: *earthquake-induced landslides*, *susceptibility assessment*, *heuristic method*, *statistical evaluation*, *cluster analysis*, *Central Italy*

1. Introduction

Hazard and risk related to landslide events have become a topic of major interest in recent years, given the growing awareness of concomitant socio-economic implications as well as environmental degradation, climatic change, rapid population growth, and improper land use (Aleotti & Chowdhury, 1999; Salvati et al., 2010; Konovalov et al., 2019; Nowicki Jessee et al., 2020).

It is widely recognised that slope instability is linked to the combination of geological, geomorphological, and climatic factors with triggering mechanisms generally ascribable to extreme weather events, seismic inputs, and anthropic activities (Guzzetti et al., 2005; Carabella et al., 2019, 2020; Livio & Ferrario, 2020; Esposito et al., 2021). Among these, seismic shaking can induce relevant changes in the landscape, leading to coseismic and post-seismic phenomena such as landslide

events. These can occur with sizes ranging from small, shallow failures in soil to large, deep rock avalanches, along with phenomena responsible for extensive damages and many casualties, as shown by several historical and recent earthquakes (Miccadei et al., 2010; Livio & Ferrario, 2020; Martino et al., 2020; Pace et al., 2020; Oswald et al., 2021). Furthermore, Earthquake-Induced Landslides (EILs) are generally responsible for severe damages and losses, as demonstrated by last decadal records when more than 50% of total worldwide losses due to landslides are associated with coseismic slope failures (Keefer, 1984, 2002; Crescenti et al., 1984; Petley, 2012; Fan et al., 2019; Martino et al., 2020). Remarkably, over the past years, the use of Geographical Information Systems (GIS) and pioneering remote sensing techniques have considerably improved our ability to map earthquake-induced landslides and to schedule activities for land defence, protection, and management (Hasegawa et al., 2009; Bozzano et al., 2010; Marchesini et al., 2014).

Landslide susceptibility is identified as the propensity of landslide events to occur in a given area, regardless of whether such events have already taken place or not. In detail, it can be defined as the estimate of the likelihood that a landslide phenomenon happens in a specific area based on local geomorphological conditions, without any statement about when it could happen (Varnes, 1984; Guzzetti et al., 1999; van Westen et al., 2006). A review of the existing literature regarding its evaluation criteria results in several approaches, depending on the final purpose and the scale of analysis, integrated with GIS techniques for the realization of thematic data layers, the computation and integration of controlling factors and data, and the assignment of weights. These various procedures can be generally classified into three main groups: heuristic, statistical, or deterministic methods (Fell et al., 2008; Rapolla et al., 2012; Marsala et al., 2019). Concerning statistical methods, in recent years several approaches have been developed based on multivariate statistics or artificial neural networks, which are becoming increasingly important also in the analysis and prediction of earthquake-induced ground effects and represent a valuable tool since they can provide objective results (Martino et al., 2019; Amato et al., 2021). These studies have been conducted based on either detailed post-earthquake field investigations, aimed at producing comprehensive EILs inventories, or

catalogues already available for the analysis, allowing a better evaluation of the role played by predisposing factors on EILs occurrence at different scales.

Within this general framework, landslide susceptibility maps exert an undeniable role since, in addition to containing relevant information on the current geomorphological instability condition of an area, depict its tendency to collapse in a probabilistic way (Guzzetti et al., 2006; Cascini, 2008). Areas of interest are usually divided into sectors sharing comparable susceptibility values and labelled according to them. Sometimes, the effort of making the understanding of the map quite immediate for the reader can lead to the identical classification of regions belonging to different areas while having different degrees of susceptibility - e.g., two or more regions can be labelled as "Highly susceptible" for having the highest susceptibility values detected in areas they belong to, regardless of whether or not their actual susceptibility degrees are comparable. Furthermore, for a given area available EILs inventories do not necessarily feature the completeness and the accuracy required for a good-quality statistical susceptibility evaluation.

Therefore, it is necessary to develop a repeatable methodology able to produce comparable results over different regions independently of the presence or absence of suitable landslide catalogues. Accordingly, in this paper, a heuristic approach for the assessment of EILs susceptibility is proposed, with the aim of detecting landslide detachment prone sectors and categorising them based on their susceptibility degree. Achieved results are then statistically analysed to provide a meaningful data classification; an example of its application to the Abruzzo Region in Central Italy is therefore presented. The work could constitute an important methodological tool for the implementation of land planning and loss-reduction measures and contribute towards the determination of situations that could lead to hazards (such as landslides) following an earthquake. Finally, it shows that accurate and multidisciplinary methodological approaches can provide important information, readily available for local administrations and decision-makers, for the implementation of sustainable land planning, emergency management, and buildings or structures design.

2. Study area

2.1 Geological and geomorphological setting

The Abruzzo Region is located in the central-eastern part of the Italian peninsula. The landscape is characterised by three main orographic and morphostructural domains: the Apennine chain area, the piedmont area, and the coastal plain (D'Alessandro et al., 2003). The chain area is characterised by a series of mountainous ridges NW-SE aligned with elevations stretching from 1000 to 2900 m above mean sea level (a.m.s.l.); wide valleys and intermontane basins are often interposed (i.e., Fucino Plain, Sulmona Basin). The chain consists of pre-orogenic carbonate lithological sequences relating to different Mesozoic-Cenozoic structural domains comprising sequences with different thicknesses, rheology, and erodibility. The bedrock of the main ridges of the Abruzzo Apennines consists of carbonate shelf, slope, and pelagic basin facies, while pelagic sequences are widespread outcropping in the Molise Apennines consisting of a chaotic assemblage on clayey-marly-limestone units; locally Quaternary continental deposits, consisting of alluvial, marshy, detrital, and eluvial-colluvial deposits occur (Parotto et al., 2004; D'Alessandro et al., 2008; Piacentini & Miccadei, 2014; Miccadei et al., 2017). The chain sharply decreases down to the piedmont area (stretching from ~600 to ~300 m a.m.s.l.), which features a cuesta and mesa landscape gently sloping towards the Adriatic Sea and incised by SW-NE river valleys. It is mainly composed of sin- and late-orogenic deposits constituted by pelitic-arenaceous turbiditic foredeep sequences, which are often covered, with the presence of erosional surfaces, by clay, sand, and sandstone of hemipelagic sequences with conglomerate levels (Ascione et al., 2008; Bigi et al., 2013). The coastal area is characterised by a sub-horizontal clayey-arenaceous-conglomeratic sequence affected by regional uplift, with elevations ranging from 0 to 300 m a.m.s.l.; the landscape is constituted by shores (80%) and steep rocky sectors (20%), and is shaped by fluvial, slope, and coastal processes that have combined thus producing a plateau and mesa relief (Figure 1; Calista et al., 2019; Miccadei et al., 2019).

The major tectonic elements are represented by N-S to NW-SE-oriented thrusts, which influenced the chain morphostructural sector from the Late Miocene to the Early Pliocene. This tectonic phase caused the tectonic units' complex superimposition, one above the other and above the syn-orogenic turbiditic sequences. This tectonics phase was followed by strike-slip tectonics characterised by NW-SE to NNW-SSE-oriented faults largely disguised by subsequent extensional tectonics. Subsequently, the orogen underwent regional uplifting since the Early Pleistocene that, in connection with local extensional tectonics affecting the chain area, caused the uplifting of the chain system, the formation of the intermontane basins, and the emersion of the Adriatic Piedmont (Figure 1; D'Agostino et al., 2001; D'Alessandro et al., 2003; Parotto et al., 2004; Patacca et al., 2008; Miccadei et al., 2012; Sembroni et al., 2020).

In this context, the geological, structural, and geomorphological setting of the region is the consequence of a complex cyclical evolution that happened in subsequent phases with the leading role of morphostructural features related either to the conflicting tectonic movements and regional uplifting or to drainage network linear down-cutting and slope instability processes (Demangeot, 1965; Bigi et al., 1995; Miccadei et al., 2017). In the inner sectors, processes and landforms mainly result from the slope gravity, surface water, karst activity, and litho-structural setting. Slope gravity processes involve the main slopes of ridges, with the formation of debris cones and talus slopes at their feet. Landslide events are widespread, with typologies influenced by the lithological and morphostructural settings: falls, topples, and debris flows along the carbonate ridges; slides and earthflows in areas where terrigenous successions outcrop (D'Alessandro et al., 2003; Carabella et al., 2019; Calista et al., 2020); also karst landforms widely characterise the region, mainly affecting the chain area and its carbonate ridges (Miccadei et al., 2018). Structural landforms (structural surfaces and scarps, ridges alignments, cuestas, hogbacks, etc.), gravitational processes (i.e., rotational and translational slides, complex landslides), and fluvial landforms (alluvial fans and terraces, badlands, gully erosion) mainly characterise the piedmont area (D'Alessandro et al., 2008; Della Seta et al., 2008; Carabella et al., 2021; Esposito et al., 2021). In the coastal sector, marine

landforms prevail with steep cliffs and wide shores interested by intense geomorphological processes controlled by the morphostructural setting. These processes are primarily represented by erosive processes, new landslides in correspondence of vertical rocky coasts, and local reactivations of ancient landslides (Calista et al., 2019; Miccadei et al., 2019).

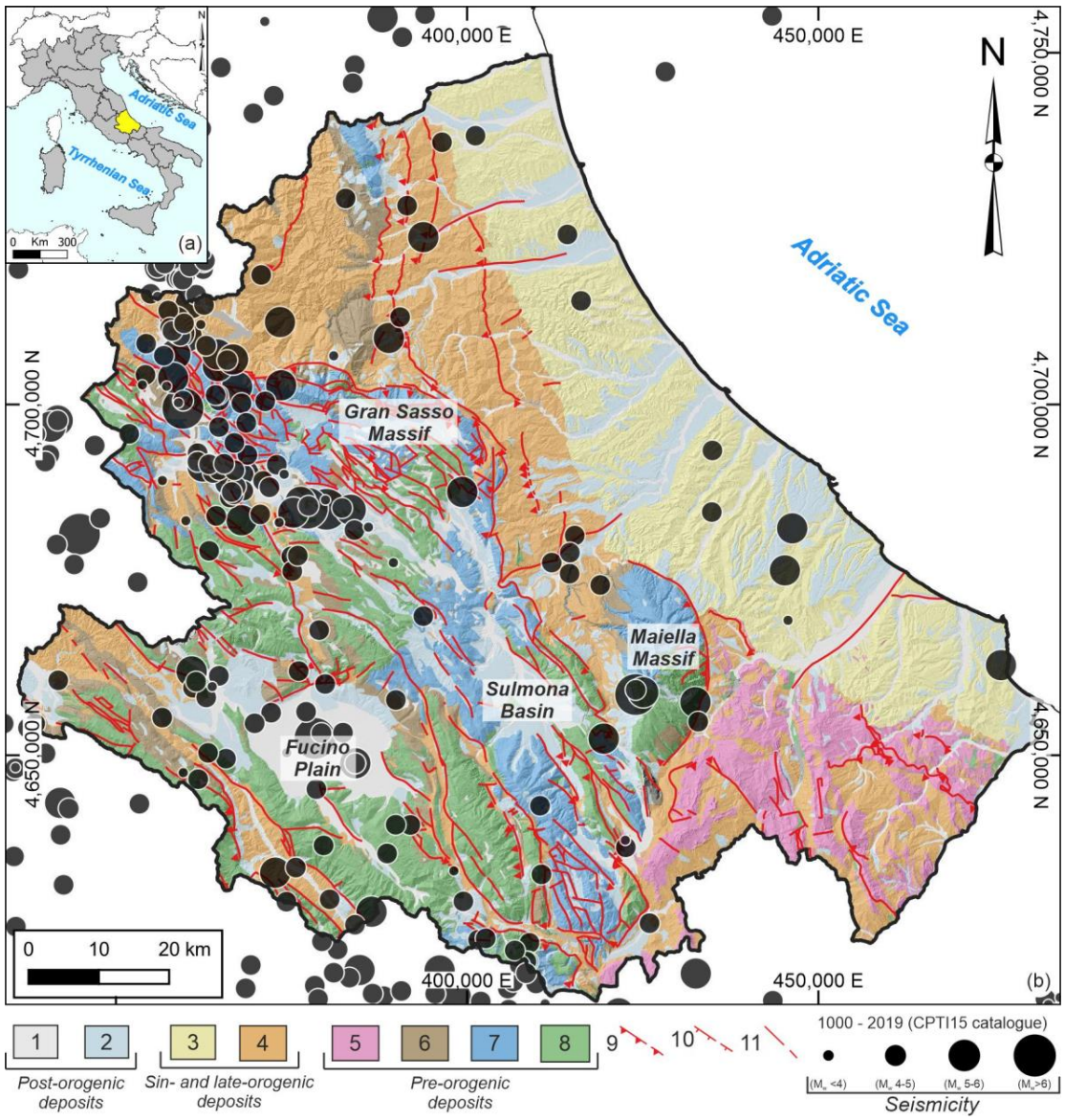

Figure 1. (a) Location of the Abruzzo Region in Central Italy; (b) Geological sketch of the Abruzzo Region. Legend: post-orogenic deposits - (1) actual fluvial deposits (Holocene), (2) old/terraced fluvial and alluvial fan terraced deposits (Middle-Late Pleistocene); sin- and late-orogenic deposits - (3) clay, sand, and sandstone of hemipelagic sequences with the presence of conglomerate levels (Late Pliocene-Early Pleistocene), (4) pelitic-arenaceous turbiditic foredeep sequences (Late Miocene-Early Pliocene); pre-orogenic deposits - (5) clay-marl-limestone of the Molise pelagic sequences (Oligocene-Miocene), (6) carbonate ramp limestones (Early Miocene- Early Pliocene), (7) slope and pelagic

basin limestones and marls (Cretaceous-Miocene), (8) carbonate platform limestones (Jurassic-Miocene); (9) main thrust (dashed if buried); (10) main normal fault (dashed if buried); (11) main fault with strike-slip or reverse component (dashed if buried); seismicity -CPTI15 (Rovida et al., 2021) catalogue (black circles).

2.2 Seismicity

The seismicity of the study area must be contextualised in the general framework of the Central Apennines, where several earthquakes are documented by historical sources since the beginning of the 19th century (i.e., Baratta, 1901 and, more recently, Valensise et al., 2020) and listed in the historical and instrumental catalogues (ISIDe Working Group, 2007; CFTI5Med, Guidoboni et al., 2019; CPTI15, Rovida et al., 2021). The seismic activity has been used for defining the seismotectonic framework of the area (i.e., Boncio et al., 2009; Vannoli et al., 2012) while active tectonic studies on the different fault systems allow the identification of the related seismogenic sources (Basili et al., 2008; DISS Working Group, 2018). The present-day tectonic setting is dominated by extension, active in the axial part of the chain (e.g., Carafa et al., 2020), which is also the area characterised by the most intense seismicity and strongest historical earthquakes (up to M 7.0; e.g., Majella Massif, 1706; Fucino, 1915; L'Aquila, 2009; Central Italy 2016-2017). Conversely, the Adriatic piedmont and the offshore area are characterised by moderate seismicity in a compressional domain on the outer thrust fronts of the central Apennines belt and along E-W shear zone cutting through the Adriatic lower plate crust (Figure 1; Fracassi and Valensise, 2007; Di Bucci & Angeloni, 2013; Kastelic et al., 2013; DISS Working Group, 2018).

According to this seismotectonic framework, the Abruzzo Region suffers mainly the shaking effects induced by strong earthquakes that enucleate along the axial zone of the Apennines and in neighbouring areas of Central Apennines, as clearly observed during the 2016-2017 Central Italy seismic sequence (e.g., Luzi et al., 2017). However, in the Adriatic piedmont also lower magnitude and shallower earthquakes may locally induce high shakings (see, for example, the 2002 Molise earthquake; Gorini et al., 2004).

2.2.1 *Earthquake-Induced Landslides (EILs)*

In the last decades, detailed geomorphological analyses have shown that the Abruzzo Region is severely affected by EILs, linked to the extreme dynamics of the area. The distribution, mechanisms, and typology of mass movements are strictly related to the different physiographic and geological-structural settings. In detail, EILs in the chain area are mainly comprised of rockfalls, occurring especially on calcareous slopes, and minor earth slides, debris and earthflows, snow avalanches, and cavity collapses; in piedmont or coastal areas, on the other side, they are mainly comprised of rockfalls on scarps set on Quaternary clayey-sandy and conglomeratic deposits, by earth slides/flows, and by anthropogenic sinkholes collapse, occurring especially in urban areas (Blumetti et al., 2009; Miccadei et al., 2010; Piacentini et al., 2013, 2020; EMERGEO Working Group et al., 2016).

The analysis of available catalogues of earthquake-induced effects allowed the reconstruction of their spatial and temporal distribution in the Abruzzo Region; in particular, the CEDIT catalogue (Italian catalogue of earthquake-induced ground failures - Fortunato et al., 2012; Caprari et al., 2018) contains more than 150 earthquakes and about 2000 earthquake-induced effects, which affected almost 1100 locations; this catalogue was recently updated with the Central Italy seismic sequence which occurred in 2016-2017. The catalogue is created on the basis of a detailed investigation of historical documents as well as on the analysis of numerous scientific papers. The analysis of documented earthquake-induced effects reveals that most of them concern landslides, being about half of the total incidents (44%). The EEE catalogue (Earthquake Environmental Effects catalogue - Guerrieri, 2015) aims to collect the wealth of information of geological and environmental effects caused by seismic events; it is composed of tables with information at site of each EEE, especially ground effects features. This database was updated with the 2016-2017 Central Italy seismic sequence, too. Finally, the landslide inventory map of the Abruzzo Region (Abruzzo Region, 2011) includes the definition, recognition, and detailed cartography of different types of landslides. It contains several EILs, most of which consequent to the L'Aquila seismic event of April 6, 2009. A total of 446 EILs were extracted from the analysis of the catalogues and categorised according to the landslide kinematics (Figure 2).

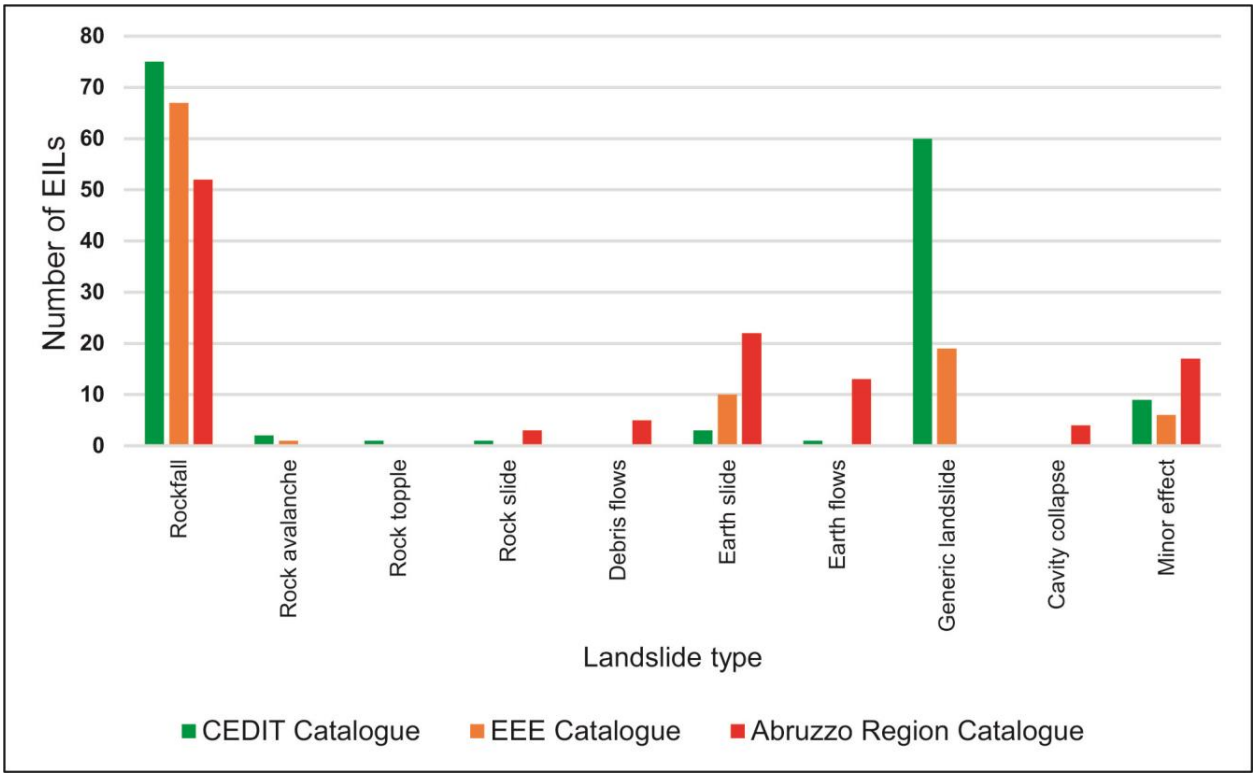

Figure 2. Bar chart showing the distribution of the type of EILs for each analysed catalogue (Abruzzo Region, 2011; Fortunato et al., 2012; Caprari et al., 2018; Guerrieri, 2015) over the Abruzzo Region.

3. Materials and methods

Earthquake-Induced Landslides (EILs) susceptibility analysis was performed through an integrated approach based on the combination of morphometric, geological, and geomorphological parameters derived from literature and field-based data, along with the critical evaluation of existing EILs catalogues, supported by multidisciplinary analyses and GIS-based techniques. In particular, a heuristic approach was applied in order to assess a preliminary EILs susceptibility map with a cell size of 10 m; resulting values were then statistically analysed to ensure a meaningful susceptibility classes definition.

3.1 Landslide-triggering parameters: detection and analysis

Statistical methods aimed at landslide susceptibility assessment require wide, complete, and temporally extended landslide inventories (Xu, 2015). Regretfully, with respect to the aim of this work, catalogues available for the study area feature substantial limitations, which make a statistical

evaluation actually unfeasible. First and foremost, events localization is not accurate enough to distinguish sectors with different susceptibility degrees at this scale of analysis. Events such as rockfalls, though occurred and detected recently, are often mapped in correspondence of accumulation areas instead of detachment zones (Figure 3a). In the case of statistical analysis, this would result in a misleading sectors classification, with detachment and accumulation areas given, respectively, a lower and a higher susceptibility degree with respect to their actual one, in strict contrast with the purpose of this study. It should be stressed that smaller-scale studies, however, could be effectively conducted following this approach, since the spatial difference between detachment and accumulation zones would not affect the final result (Amato et al., 2021). Another aspect to consider is that different landslides are sometimes mapped as a single event when occurring in a small area, with a subsequent wrong susceptibility degree evaluation (Figure 3b). Finally, detailed data of non-recent events are definitively missing, with mapped EILs often featuring poor geographical and chronological constraints (Figure 3c).

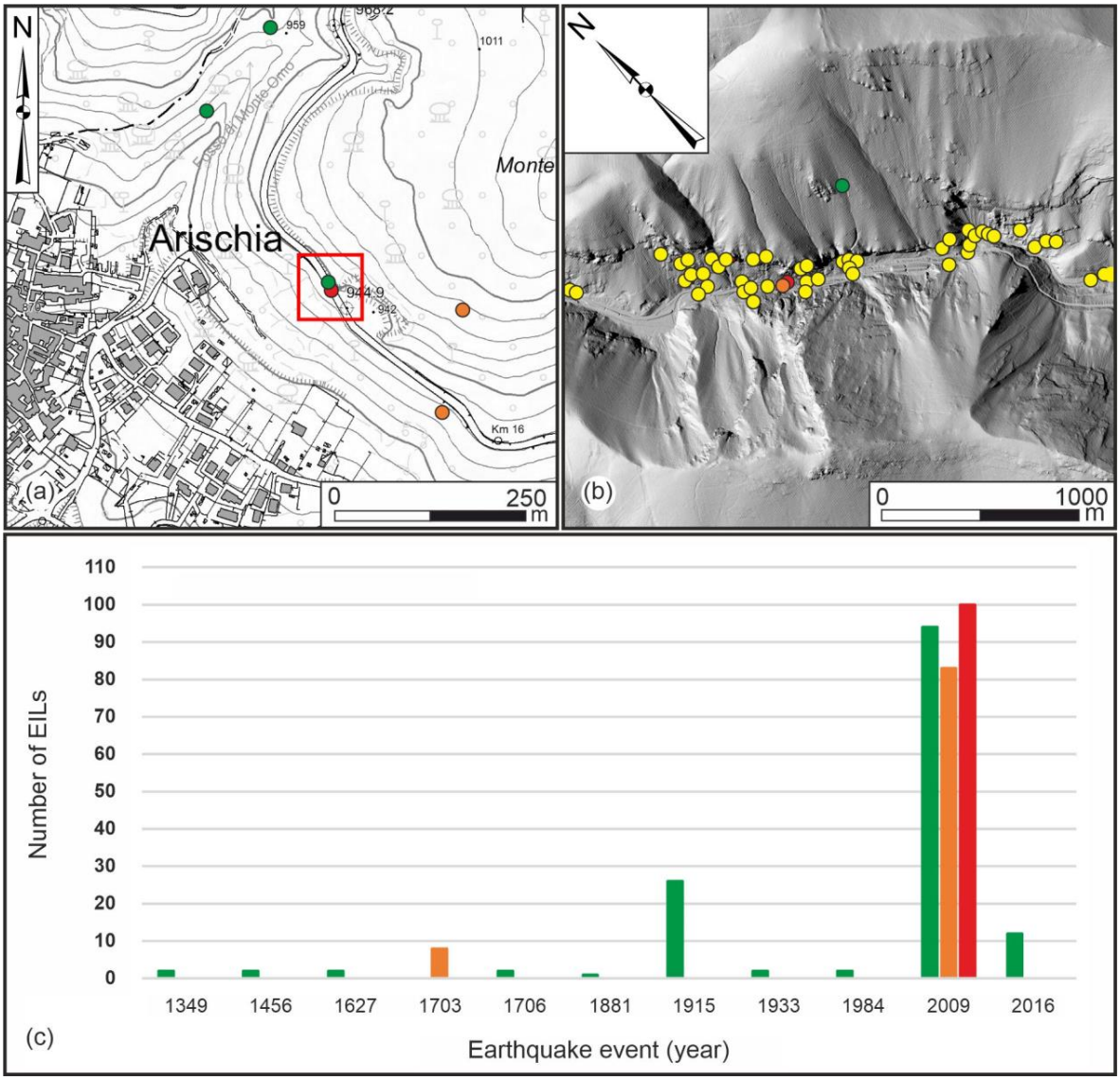

Figure 3. EILs events reported on CEDIT (green dots and bars; Caprari et al., 2018), EEE (orange dots and bars; Guerrieri, 2015), and Abruzzo Region (red dots and bars; Abruzzo Region, 2011) catalogues. Yellow dots refer to earthquake-triggered rockfall blocks in the area of San Venanzio gorges (Raiano, AQ) according to Piacentini et al., 2013. (a) Example of events mapped in correspondence of accumulation areas (roads) instead of detachment zones (red box); (b) example of multiple events mapped as a single event; (c) number of EILs per event showing a clear lack of available data for non-recent earthquakes.

For these reasons, given the available data, in this study a heuristic approach appears to be highly preferable to a statistical one. Heuristic methods require the combination of several parameters that contribute to slope instability. Each of these parameters and their spatial variability, represented through thematic maps, are, in turn, analysed and subdivided into a suitable number of classes.

Subsequently, each of these parameters is given a certain weight, based on expert judgment, and according to the influence exerted on landslide susceptibility derived by critically analysing literature data and available EILs catalogues (Abruzzo Region, 2011; Guerrieri, 2015; Caprari et al., 2018). From the algebraic sum of the weights associated with individual parameters, a final map is constructed wherein high/low numerical values correspond to a high/low propensity of the slope to fail (Ruff & Czurda, 2008; Magliulo et al., 2009; Pourghasemi et al., 2018; Reichenbach et al., 2018). The selection of factors strictly depends on available data concerning the object and the aims of the study. In this paper, each factor described in the following paragraphs was chosen to better match the variability of the data source and to outline its role in the landslide mechanism in the geological, structural, and geomorphological framework of the region. The nine different factors considered for the present landslide susceptibility analysis are: slope, aspect, topographic curvature, outcropping lithofacies, degree of rock fracturing, karst incidence, distance from active faults, distance from earthquake epicentres, and presence of anthropogenic sinkholes. The choice of these parameters was also dictated by the scale of analysis, since for studies of higher detail the integration of local-scale factors both of natural and anthropogenic origin is advisable (e.g., slopes undercutting by erosion or artificial excavation; Chigira & Yagi, 2006; Martino et al., 2019). Finally, although Peak Ground Acceleration (PGA) values are available for the study area through the MPS04 seismic hazard map of Italy (Stucchi et al., 2004), they were not considered to not overestimate the contribution of seismic parameters, already implemented by accounting for distances from active faults and earthquake epicentres.

Morphometric parameters, i.e., slope, aspect, and topographic curvature, are all derived from a 10 m resolution Digital Terrain Model (DTM) available at the opendata.regione.abruzzo.it web page, by means of ESRI ArcGIS™ 10.6 tools.

Slope, expressed as an angle [°] to the horizontal, is commonly used in landslide susceptibility analysis. An increase in its gradient usually corresponds to an increase in hillside instability (Çevik & Topal, 2003; Yalcin et al., 2011).

277 **Topographic curvature**, expressed in [m^{-1}], is computed along the direction of the maximum slope.
278 The parameter is taken into account in terms of the control it exerts on ground shaking; in particular,
279 a convex surface leads to a focusing of seismic waves, which increases acceleration; a concave surface
280 induces the dispersion of waves and, consequently, an acceleration decrease (Pischiutta et al., 2017;
281 Maufroy et al., 2018). In this work, topographic curvature (Tc) values are divided into three ranges,
282 $Tc \leq -0.5$, $-0.5 < Tc \leq 0.5$, and $Tc > 0.5$, indicating, respectively, concave, planar, and convex
283 surfaces (Pham et al., 2017).
284 **Aspect**, expressed as a cardinal direction, is considered less important compared to other parameters
285 (Carrara et al., 1991; Çevik & Topal, 2003); nevertheless, it is generally taken into account due to its
286 connection to the microclimate acting on slopes and the consequent weathering (Komac, 2006;
287 Shahabi et al., 2014). According to many authors, it is assumed that such processes act more
288 effectively on south-facing slopes due to pronounced temperature variations and higher humidity
289 (Capitani et al., 2013; Pham et al., 2017).
290 **Lithology** has a great influence on landslide susceptibility (Carrara et al., 1991; Çevik & Topal, 2003;
291 Shahabi et al., 2014; Esposito et al., 2021). A Lithofacies map of the Abruzzo Region was hence
292 created through digitisation of the 1:250.000 scale Lithofacies map of Latium-Abruzzo and
293 neighbouring areas (Accordi & Carbone, 1988). Missing sectors were included after analysis and re-
294 adaptation of the 1:100.000 scale Geological map of Abruzzo (Vezzani & Ghisetti, 1998) and the
295 1:50.000 scale Geological sheets of the CARG Project available for the study area (ISPRA, 2017).
296 Units resulting from this process were joined into17 lithological units based on the sedimentation
297 environment and the lithological features of the outcrops. The impact on landslide susceptibility of
298 each group is assessed by analysing the distribution of the main landslides (ISPRA, 2007; Abruzzo
299 Region, 2019). It was also based on EILs density, which was computed for each lithological unit by
300 accounting for inventoried events (Abruzzo Region, 2011; Caprari et al., 2018; Guerrieri, 2015).
301 The **degree of rock fracturing** results from the interaction between the lithological features of
302 outcrops and the regional tectonics (ISRM, 1978; Sperrevik et al., 2002; Molnar et al., 2007). This

parameter exerts a clear influence on landslide susceptibility, and it is often used to detect failure mechanisms and define the landslide geometry, showing higher values linked to a greater slope instability (ISRM, 1978; Barisone et al., 1994).

Karst phenomena deeply affect rock mechanical properties by inducing the calcium carbonate dissolution and the subsequent formation of natural caves prone to collapse in response to seismic shaking (Santo et al., 2007; Pace et al., 2020). Different sectors were distinguished based on their lithological features, the presence of natural caves (Abruzzo Region, 2011), and the karst state of activity. A higher karstification degree is associated with a greater landslide susceptibility.

The **distance from active faults** exerts a major control on earthquake-induced landslide susceptibility of a region, as empirically shown by the rapid decrease of EILs events moving away from the surface traces of faults connected to the attenuation of the seismic input (Xu & Xu, 2014; Shao et al., 2019). Detection and digitisation of faults were based on the ITHACA catalogue (ITaly HAzard from CApable faults - Michetti et al., 2000; ITHACA Working Group, 2019) implemented with Boncio et al. (2004). Areas located at different distances from faults traces are detected using the Buffer tool implemented in ArcGIS^{TM} 10.6. Hanging walls and footwalls were differentiated, given the higher density of EILs usually occurring above the fault plane (Martino et al., 2014); consequently, two different rasters were created. In this paper, fault systems located in neighbouring regions are also considered, given their contribution to the landslide instability of the Abruzzo Region (Villani et al., 2018).

By analysing landslide movements in the first years after an earthquake, many authors detected a close correlation between the number of mass movements and the proximity to epicentral zones (Martino et al., 2014; Zhang et al., 2016; Yang et al., 2017; Shao et al., 2019). The **distance from epicentres** was therefore computed using the Euclidean distance tool implemented in ArcGIS^{TM} 10.6. Only events with a $4.0 < Mw < 6$ were considered in the analysis since lower magnitudes rarely trigger landslides (Keefer, 1984), whereas higher magnitudes refer to infrequent events that are unrepresentative of the actual seismicity of the area (Rovida et al., 2021). It is widely recognised that

329 an increase of the magnitude corresponds to an increase in the area prone to EILs (Keefer, 2002). For
330 a correct assessment of landslide susceptibility related to the epicentral distance, seismic events were
331 thus divided into four equally spaced classes based on related Mw; consequently, four different
332 thematic maps were created. Each class is also corrected by a factor stating the epicentres density
333 using the Kernel density tool with a radius of 10 km. As for the distance from active faults, epicentres
334 falling into neighbouring regions are taken into consideration. Weights are were then assigned based
335 on literature-accepted relations between epicentral distances of landslides and earthquake magnitudes
336 (Keefer, 1984, 2002).
337 Finally, **anthropogenic sinkholes** were considered. They have a consistent role in arising the EILs
338 hazard, given their presence in areas often heavily urbanised (Fiore & Lanzini, 2007; Nisio et al.,
339 2007). Their detection and digitisation were based on the Geohydrological Plan (Abruzzo Region,
340 2011), properly integrated with the ISPRA Sinkhole catalogue (ISPRA, 2020). Areas of attention
341 were defined by setting a buffer zone around mapped sinkholes with a radius of 500 m.
342 The above listed parameters were therefore classified following a heuristic approach and given proper
343 weight, based on literature data as well as on the critical evaluation of available EILs inventories
344 (Table 1).

345 **Table 1.** Parameters analysed in EILs susceptibility assessment and assigned weights.

Parameter #	Parameter	Source	Class	Weight
1	Slope [°]	DTM	0-20	0
			20-30	1
			30-35	2
			35-40	3
			40-45	5
			45-60	7
			60-70	9
			70-80	11
			80-90	12
2	Topographic curvature	DTM	Concave	0
			Planar	2
			Convex	7
3	Aspect [°]	DTM	Plain	0
			337.5-22.5 - N	0
			22.5-67.5 - NE	0
			67.5-112.5 - E	1
			112.5-157.5 - SE	2
			157.5-202.5 - S	3
			202.5-247.5 - SW	2
			247.5-292.5 - W	1
			292.5-337.5 - NW	0

4	Outcropping lithofacies	Literature (Accordi & Carbone, 1988; Vezzani & Ghisetti, 1998)	Eluvial and colluvial deposits	2
			Sandy shore deposits	0
			Recent fluvial-lacustrine deposits	0
			Travertine deposits	7
			Moraine deposits	7
			Old fluvial-lacustrine deposits	2
			Conglomerate deposits	7
			Clay-sand deposits	3
			Sand turbidites	7
			Pelite turbidites	3
			Limestone deposits in conglomeratic and calcarenitic facies	6
			Allochthonous pelagic deposits	3
			Limestones in carbonate ramp facies	10
			Limestones and marls in basin facies	7
			Limestones in slope facies	6
			Limestones in open carbonate shelf-edge facies	7
			Limestones and dolomites in carbonate shelf facies	8
5	Degree of rock fracturing	Field data and literature (Pasculli et al., 2014)	Not susceptible to fracturation	0
			Low	4
			Medium	5
			High	7
			Very high	12
6	Karst incidence	Field data and literature (Pasculli et al., 2014)	Null	0
			Inactive	1
			Low	2
			Medium	5
			High	10
7	Distance from active faults [km] Hanging wall	Literature (Michetti et al., 2000; Boncio et al., 2004)	0 - 5	12
			5 - 10	9
			10 - 15	8
			15 - 20	7
			20 - 25	6
			25 - 35	5
			35 - 45	4
			45 - 60	3
			60 - 70	2
	Distance from active faults [km] Footwall	Literature (Michetti et al., 2000; Boncio et al., 2004)	0 - 5	9
			5 - 10	7
			10 - 15	5
			15 - 20	4
			20 - 25	3
			25 - 35	2
			35 - 45	1
			> 45	0
8	Distance from epicentres $4 \leq Mw < 4.5$	Literature (Rovida et al., 2021)	0 - 3	9
			> 3	0
	Distance from epicentres $4.5 \leq Mw < 5$	Literature (Rovida et al., 2021)	0 - 3	64
			3 - 6	15
			6 - 10	6
			10 - 12	3
			> 12	0
	Distance from epicentres $5 \leq Mw < 5.5$	Literature (Rovida et al., 2021)	0 - 3	291
			3 - 6	68
			6 - 10	27
			10 - 15	14
			15 - 20	8
			20 - 25	5
			25 - 30	4
			> 30	0
	Distance from epicentres $5.5 \leq Mw < 6$	Literature (Rovida et al., 2021)	0 - 3	1000
			3 - 6	232
			6 - 10	93
			10 - 15	47
			15 - 20	27
			20 - 25	19
			25 - 30	14
			30 - 40	11
			40 - 50	7
			50 - 60	6
			60 - 80	4
			> 80	0

9	Anthropogenic sinkholes	Field data and literature (Abruzzo Region, 2011; ISPRA, 2020)	Buffer zone (radius = 500 m)	5

346

347 The listed parameters were then subdivided into primary and secondary, based on the extension of
348 the area they affect. In this paper, only Anthropogenic sinkholes are categorised as the latter since
349 they influence a percentage of the regional territory much less than other parameters.
350 Subsequently, using the Raster Calculator tool implemented in ArcGIS™ 10.6, thematic maps
351 depicting the distance from the epicentres are all summed cell by cell, and resulting values are
352 expressed on a scale from 1 to 10 to ensure comparability with other parameters; the resulting map is
353 then summed cell by cell to weighted rasters of other primary parameters. A preliminary EILs
354 susceptibility map is thus obtained using GIS technology (*Heuristic analysis*, Figure 4).

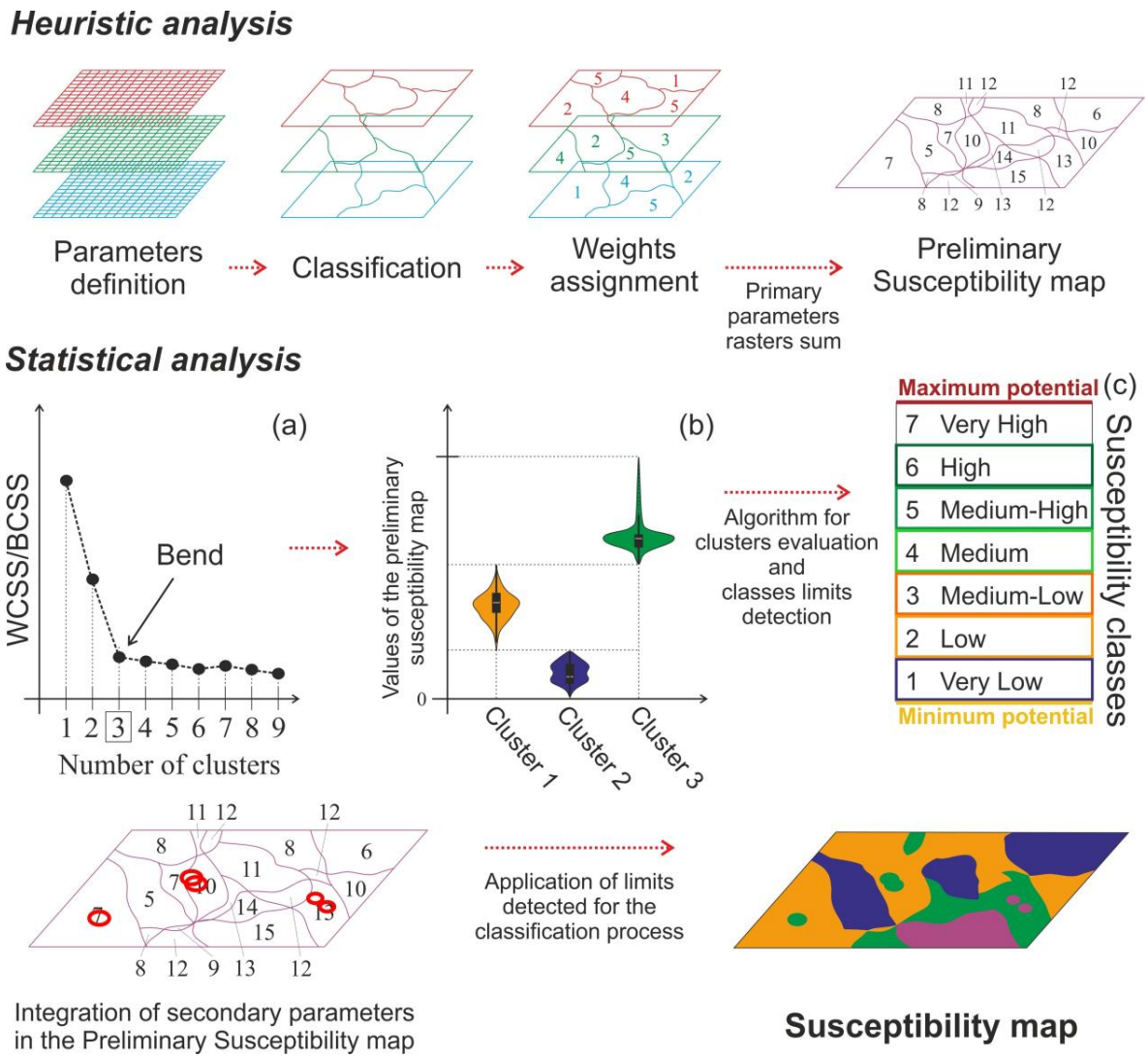

Figure 4. Workflow of the applied methodology. In the Heuristic analysis, the steps followed to get the Preliminary Susceptibility map from rasters of primary parameters are shown. In the Statistical analysis, the Elbow method, the analysis of cluster values by means of violin plot diagrams, and the detection of limits of susceptibility classes - with respect to an absolute scale and after application of the algorithm shown in Figure 5 - are presented. Finally, the integration of secondary parameters in the Preliminary Susceptibility map and the creation of the final Susceptibility map are shown.

3.2 Unsupervised classification, susceptibility classes definition, and map creation

Statistical analysis was performed after the preliminary landslide susceptibility analysis to divide the study area into an optimal number of susceptibility classes, a number that is actually beforehand unknown. In order to define it, an unsupervised classification is executed by means of kmeans R© routine (Forgy, 1965) on the preliminary map resulting from the heuristic analysis. The process groups together pixels sharing similar statistical properties into a user-specified number of distinct

clusters. For each cluster, it also returns relevant statistics, including the central value, the number of cells, and the Within Cluster Sum of Squares and, for each group of clusters, the total Within Clusters Sum of Squares (WCSS) and the Between Clusters Sum of Squares (BCSS). The preliminary susceptibility raster is hence classified into a number of groups ranging from 2 up to 7. The optimal number is finally defined through the elbow method by plotting the WCSS/BCSS ratios against the number of clusters. A bend in the plot occurs indicating the minimum number of clusters such that the total intra-cluster variation is minimised and the between-clusters variation is maximised (Tripathi et al., 2018; Mascioli et al., 2021; Figure 4a).

Statistics of clusters are analysed by plotting values of each group on violin plot diagrams, which are a combination of a box plot and a probability density function plot. They explicitly show the median, the interquartile range, the upper and lower adjacent values, and the kernel probability density of the data at different values (Wei et al., 2012; Figure 4b).

An absolute susceptibility scale is then introduced with values ranging from the minimum to the maximum potential values of the area, computed by summing the minimum and the maximum potential values of all primary parameters. By dividing the resulting range into a fixed number of equally spaced intervals, a series of meaningful classes are detected. This procedure ensures the comparability of results obtained in different areas when maximum and minimum potential values of parameters are used to build the scale (e.g. if slope values of a region range from 20 to 50°, upper and lower limits of the absolute scale should be computed by accounting also for weights associated to 0-20 and 50-90° slope classes). The application of the algorithm presented in Figure 5, i.e. the critical comparison between clusters statistics and classes of the absolute susceptibility scale, allows the definition of proper numerical limits for the final classification (Figure 4c).

The last phase of the analysis is the creation of the final Susceptibility map. In this phase, secondary parameters - previously set aside - are taken into consideration. In this work, the raster depicting the Anthropogenic Sinkholes is summed cell by cell to the preliminary susceptibility map. The resulting

raster is then classified based on limits detected through the statistical steps. Values eventually exceeding the absolute susceptibility scale are assigned to the highest level susceptibility class.

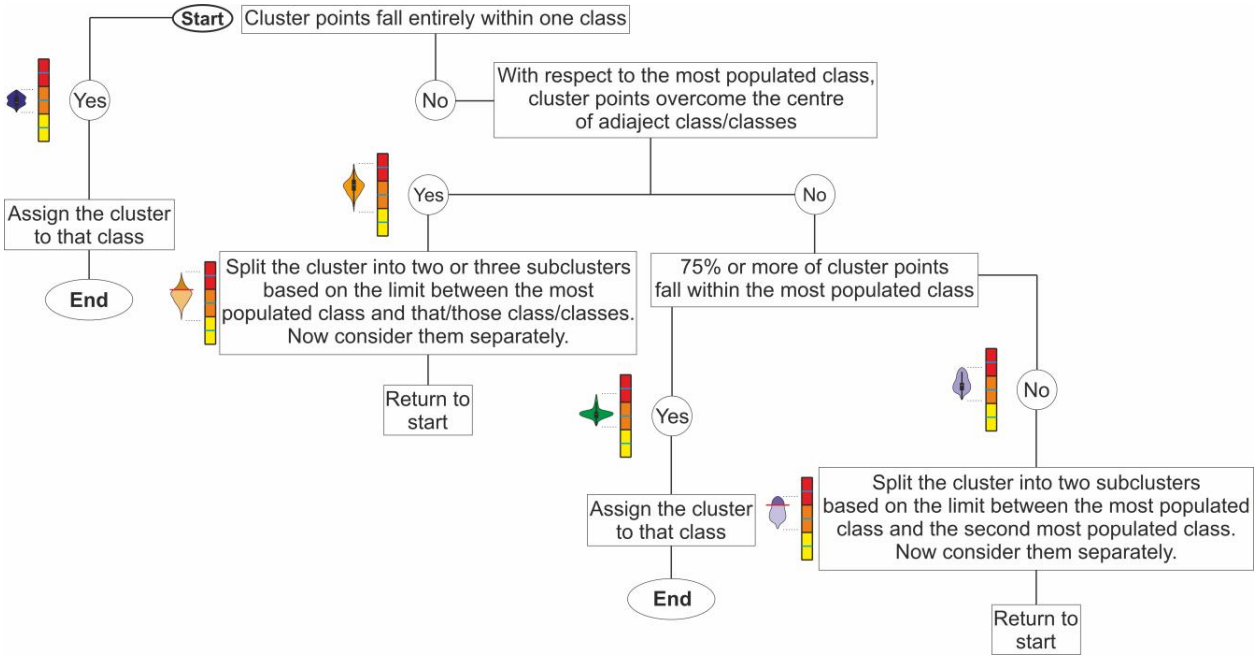

Figure 5. Flowchart showing the logical process for class detection. Steps are designed to achieve the best differentiation among classes and overcome limits intrinsic to the stand-alone unsupervised classification, such as the grouping of values representative of clearly different susceptibility degrees.

4. Results

4.1 Morphometric maps

4.1.1 Slope map

The study area shows slope values ranging from 0 up to approximately 90° (Figure 6a). Values between 0 and 5° are detected in coastal areas, alluvial valleys of piedmont areas, and intermontane basins (such as Fucino Plain and Sulmona Basin), as well as basins with a minor areal extension. Low-to-medium values (ranging from 5 to 20°) are found in the whole piedmont area and along narrow sectors surrounding the intermontane basins. Finally, values ranging from 20 to 40° characterise the chain sector corresponding to the main ridges interrupted by longitudinal and transversal valleys; slope values above 50° are mostly detected on Maiella and Gran Sasso massifs, although narrow steep sectors are locally found in ridges, gorges, and minor valleys.

409 #### *4.1.2 Topographic curvature map*

410 The surface curvature of the study area is characterised by well-defined planar surfaces,
411 characterising coastal sectors, the main alluvial plains in the piedmont area, and the intermontane
412 basins (i.e., Fucino Plain and Sulmona basin; Figure 6b). On the other hand, convex and concave
413 surfaces alternate almost regularly across the study area, depicting a mountainous and hilly landscape
414 dominated by ridges, isolated reliefs, and longitudinal and transversal river valleys.

415 #### *4.1.3 Aspect map*

416 The study area shows a clear differentiation between the chain and the piedmont/coastal sectors
417 (Figure 6c). The former is characterised by mainly NW-SE oriented slopes, in accordance with the
418 vergence of the Central Apennine chain. The latter shows an average SW-NE direction in close
419 relationship with the development of the drainage network, characterised by main fluvial valleys and
420 the small tributary catchments of main rivers and those incising the coastal slope.

THIS ARTICLE IS A PREPRINT

The published version is avaiable at: https://doi.org/10.1016/j.catena.2021.105729

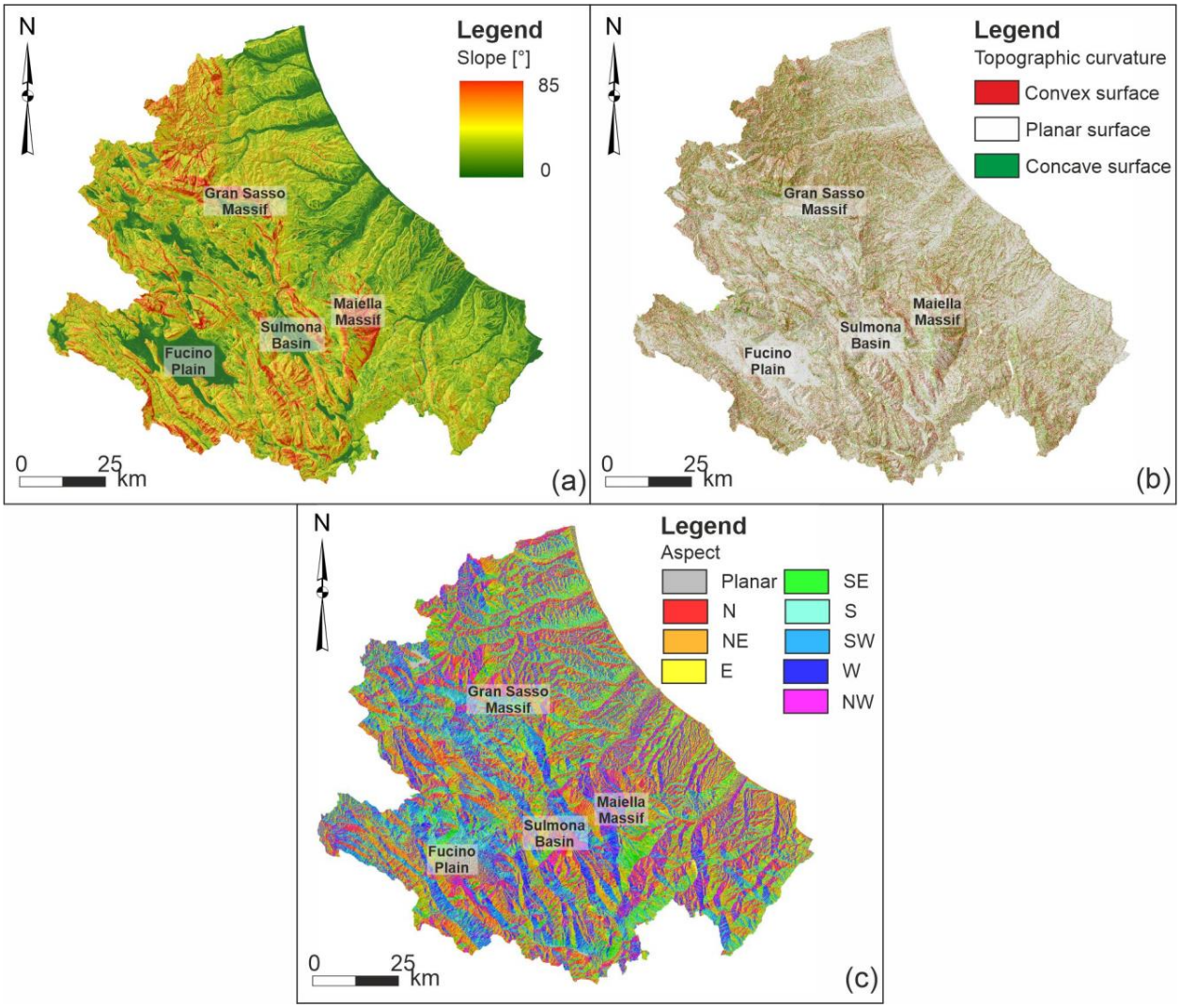

Figure 6. Morphometric maps of Abruzzo Region. (a) Slope map; (b) Topographic curvature map; (c) Aspect map.

4.2 Geothematic maps

4.2.1 Lithofacies map

From a lithological standpoint, limestones in carbonate shelf facies, limestones in slope facies, limestone and marls in basin facies characterise the major ridges of the Abruzzo Apennines (i.e., Gran Sasso Massif and Maiella Massif). Allochthonous pelagic deposits are widely outcropping in the southern areas showing a chaotic assemblage on clayey-marly-limestone units. Bedrock lithologies in the piedmont sector pertain to sand-pelite turbidites and marine clay-sand and conglomerate deposits (Figure 7). Quaternary continental deposits are extensively outcropping in the intermontane basins, alluvial valleys, and coastal sectors. They pertain to fluvial-lacustrine, travertine, sandy shore, and eluvial and colluvial deposits.

THIS ARTICLE IS A PREPRINT

The published version is avaiable at: https://doi.org/10.1016/j.catena.2021.105729

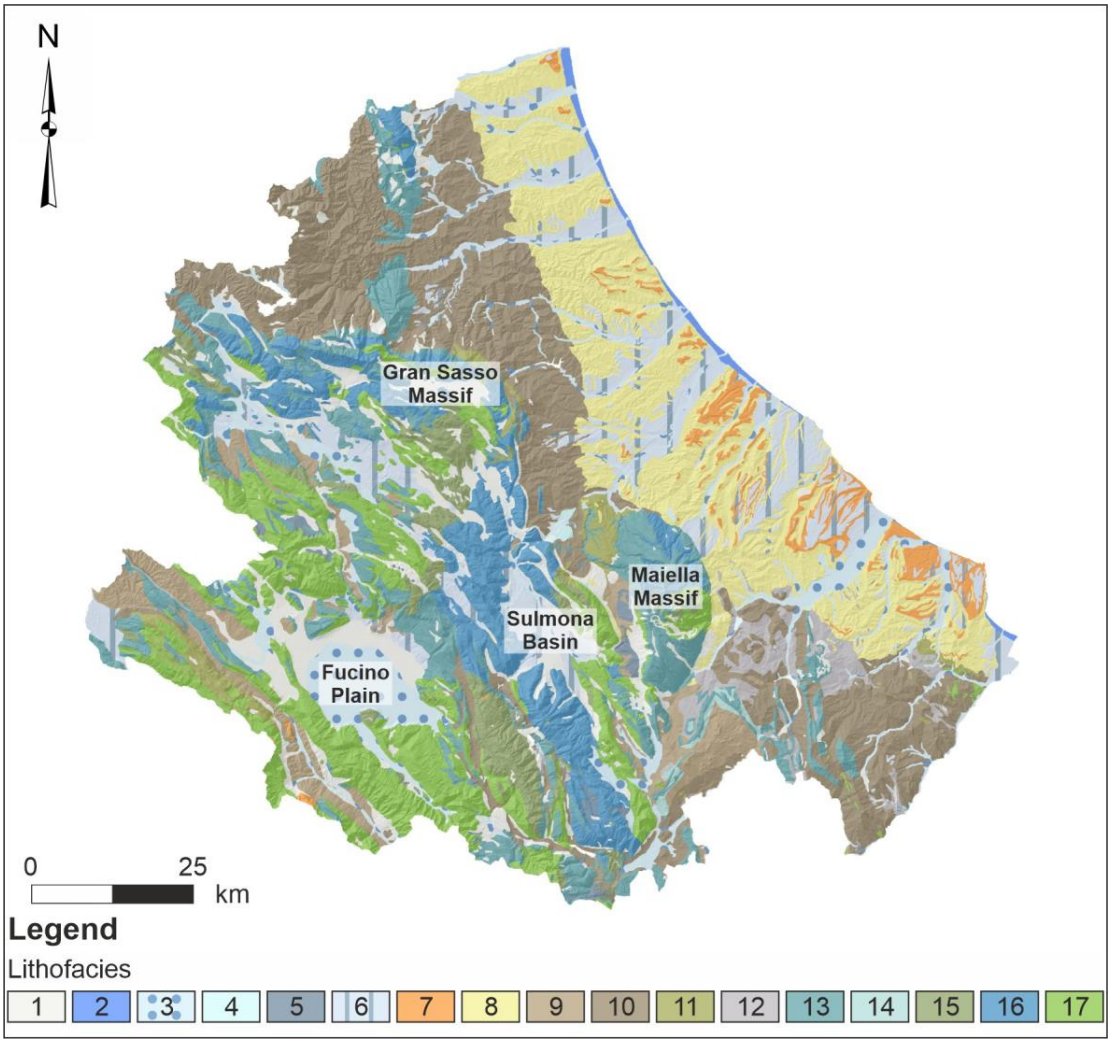

Figure 7. Lithofacies map of the Abruzzo Region (modified from Accordi et al., 1988; Vezzani & Ghisetti, 1998; ISPRA, 2017; Esposito et al., 2021). 1) Eluvial and colluvial deposits; 2) Sandy shore deposits; 3) Recent fluvial-lacustrine deposits; 4) Travertine deposits; 5) Moraine deposits; 6) Old fluvial-lacustrine deposits; 7) Conglomerate deposits; 8) Clay-sand deposits; 9) Sand turbidites; 10) Pelite turbidites; 11) Limestone deposits in conglomerate and calcarenite facies; 12) Allochthonous pelagic deposits; 13) Limestones in carbonate ramp facies; 14) Limestones and marls in basin facies; 15) Limestones in slope facies; 16) Limestones in open carbonate shelf-edge facies; 17) Limestones and dolomites in carbonate shelf facies.

4.2.2 Degree of rock fracturing map

Fractures, faults, and their patterns exert a fundamental influence on the mechanical and transport properties of rocks. According to its physiographic and geological-structural setting, the Abruzzo Region shows a heterogeneous spatial arrangement of fracture arrays. Piedmont and coastal sectors, as well as intermontane basins, are characterised by lithologies that do not have a large effect on

fracture attribute distributions. Nevertheless, there are episodic and localized slope instability processes related to morphostructural setting in weak rock hills (e.g., hog-back relief, mesa relief affected by intersecting major joints) and cliff recession processes combined with wavecut and slope gravity processes widely controlled by main joints in the coastal area (Calista et al., 2019; Miccadei et al., 2019). In these areas, outcropping weak rocks are classified as not susceptible to fracturation (Figure 8a). In detail, areas showing a low degree of fracturation are detected towards NW and in narrow sectors of the piedmont. Medium values are found along the slopes of the Maiella Massif and the Gran Sasso ridge. High and very high values, finally, characterise the carbonate sectors of the westernmost sectors of the Abruzzo Region in accordance with a general NW-SE trend of tectonic lineaments.

4.2.3 Karst incidence map

According to the lithological framework, karst incidence is completely absent in the piedmont sector and in intermontane basins (Figure 8b). Karst morphogenesis widely affects carbonate rocks outcropping in the chain area, showing the highest values on carbonate shelf successions and low-to-medium values on limestones in carbonate ramp and basin facies. Finally, inactive karst processes characterise the limestones in open carbonate shelf-edge facies, locally widespread in central and southern sectors of the region.

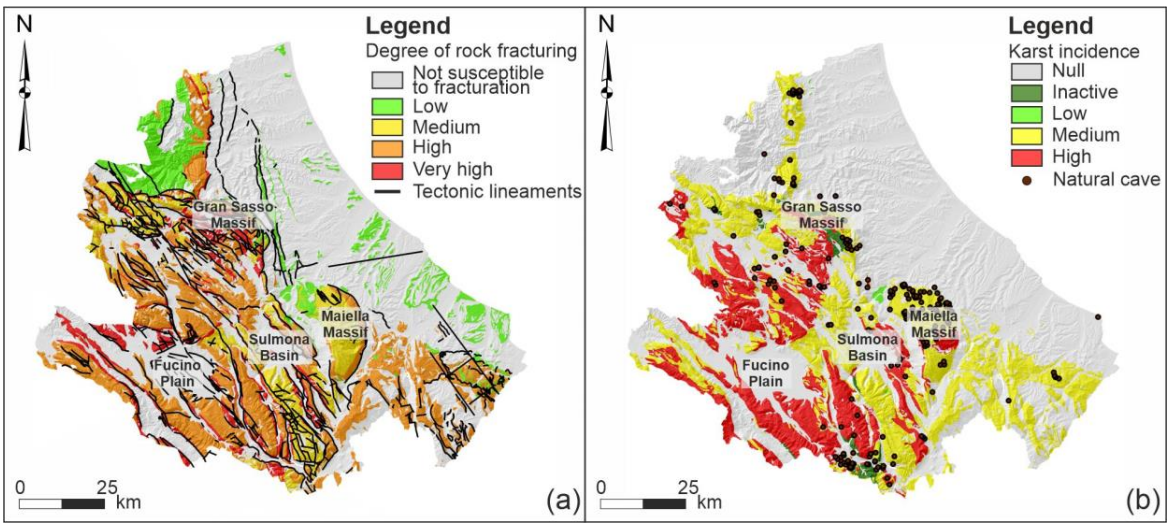

Figure 8. (a) Degree of rock fracturing and (b) Karst incidence maps (modified from Pasculli et al., 2014).

4.2.4 *Distance from active faults maps*

Thematic maps depicting the distance from active faults show values ranging from 0 up to approximately 60 km, with slight differences between hanging walls/footwalls-related maps (Figure 9). Minimum distances are detected in the chain sector according to the spatial arrangement of fault systems derived and implemented from Boncio et al. (2004) and the ITHACA Working Group (2019). Active fault systems located in neighbouring regions are also considered, taking into account their contribution to landslide instability of the Abruzzo Region as clearly observed during the 2016-2017 Central Italy seismic sequence. Maximum values are found in the external piedmont sector and along the coastal one.

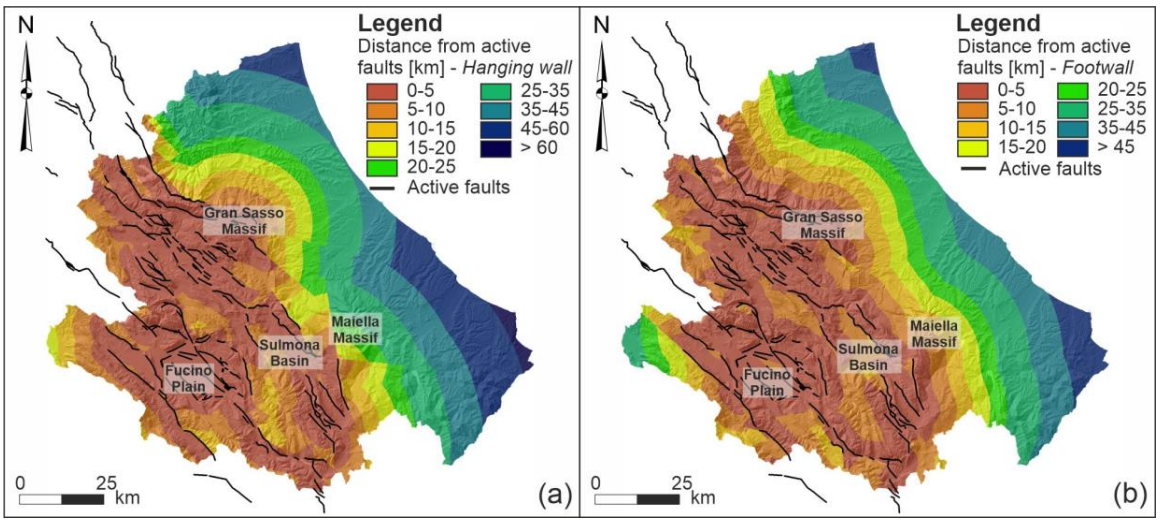

Figure 9. Distance from active faults maps: (a) hanging wall and (b) footwall.

4.2.5 *Distance from epicentres and epicentres density maps*

Maps depicting the distance from epicentres show values ranging from 0 to approximately 50 km, depending on the magnitude range (Figure 10, left column). The spatial distribution of epicentres reflects the tectonic setting of the Abruzzo Region, characterised by both historical and recent strong seismicity. The majority of epicentres related to events with $4 \leq Mw < 4.5$ falls into the chain sector, with rare events located in the central and northern piedmont/coastal area (Figure 10a, left column).

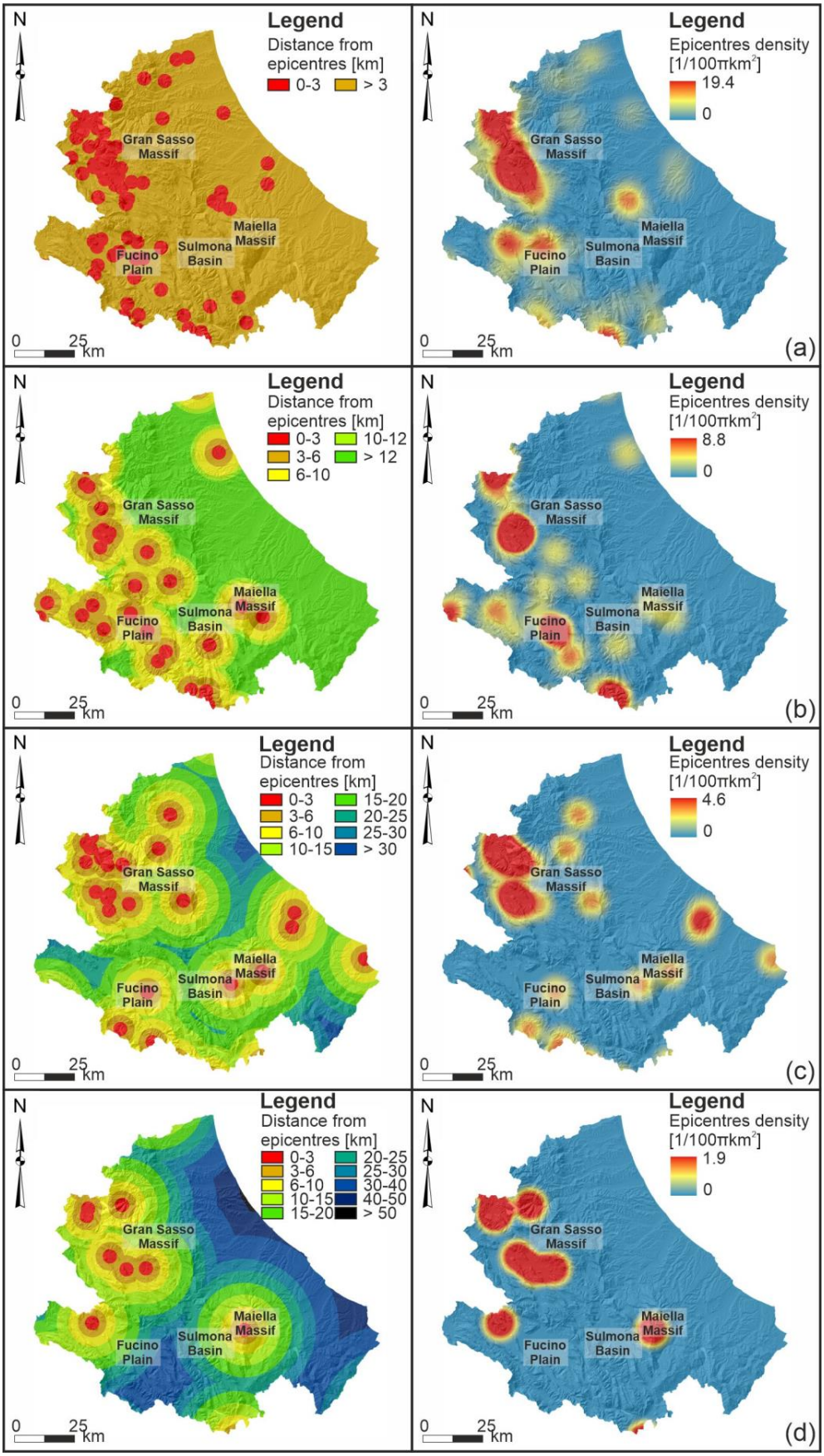

Figure 10. Thematic maps depicting distance from epicentres (left column) and epicentres density (right column) for earthquakes with a) $4 \leq Mw < 4.5$, b) $4.5 \leq Mw < 5$, c) $5 \leq Mw < 5.5$, and d) $5.5 \leq Mw < 6$.

Epicentres of earthquakes with 4.5 ≤ Mw < 5 are all located in the chain sector, except for sporadic events found in the northern piedmont/coastal area (Figure 10b, left column). Events with 5 ≤ Mw < 5.5, on the other hand, are concentrated in the north-western sector and, secondarily, in the Fucino plain and Maiella areas as well as in the central-southern piedmont/coastal sector (Figure 10c, left column). Finally, epicentres of earthquakes with 5.5 ≤ Mw < 6 are absent in the piedmont/coastal area, being mostly located in the north-western sector of the region (Figure 10d, left column). Epicentres density is graphically shown in thematic maps of Figure 10 (right column). This analysis was performed by dividing seismic events into four equally spaced classes based on related Mw, according to the georeferenced location of epicentres. Relevant values decrease is observed as related magnitude increases; the highest values, however, are always detected in the chain sector.

4.2.6 Anthropogenic sinkholes map

Anthropogenic sinkholes present a high concentration in the external sector of the chain and the piedmont/coastal area, greater in major urban areas (Figure 11).

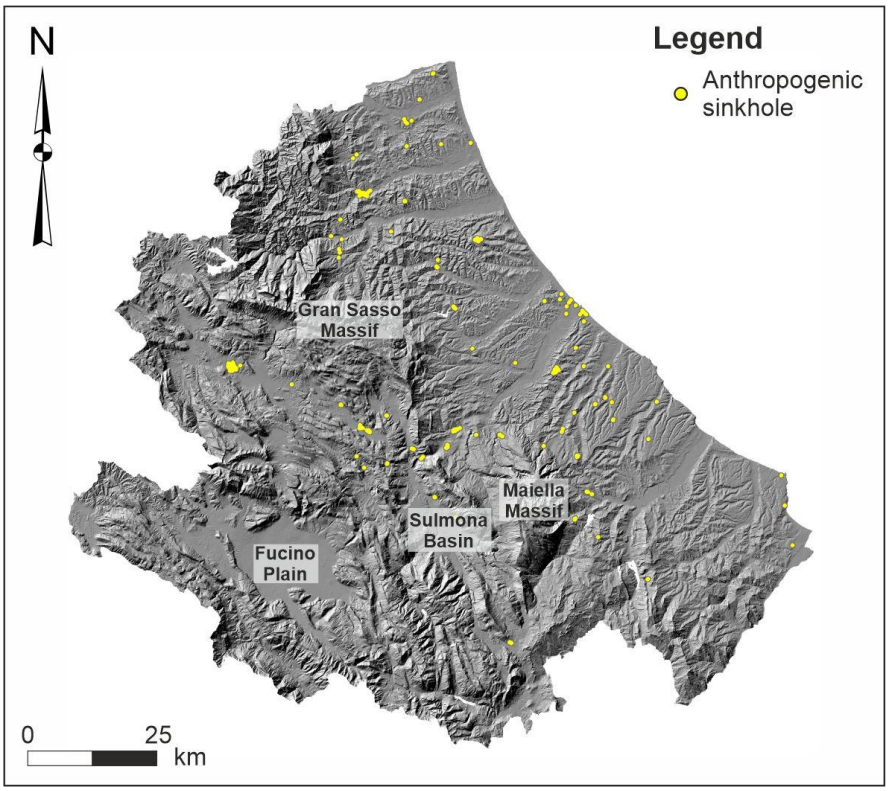

Figure 11. Anthropogenic sinkholes map.

4.3 Susceptibility map

4.3.1 Preliminary susceptibility map

The Preliminary susceptibility map shows values generally increasing moving from the coastal sector towards the piedmont and the chain ones (Figure 12). In the current analysis, different regions featuring low, medium, and high landslide susceptibility were identified. More specifically, areas characterised by low values are located in the external portion of the piedmont sector and along the coastal area. Medium values are mainly detected in the inner piedmont and intermontane basins. The highest values are located in correspondence with reliefs in the inner chain sector and the incision of main rivers. Local areas without class values present no landslide susceptibility and mostly correspond to lake surfaces.

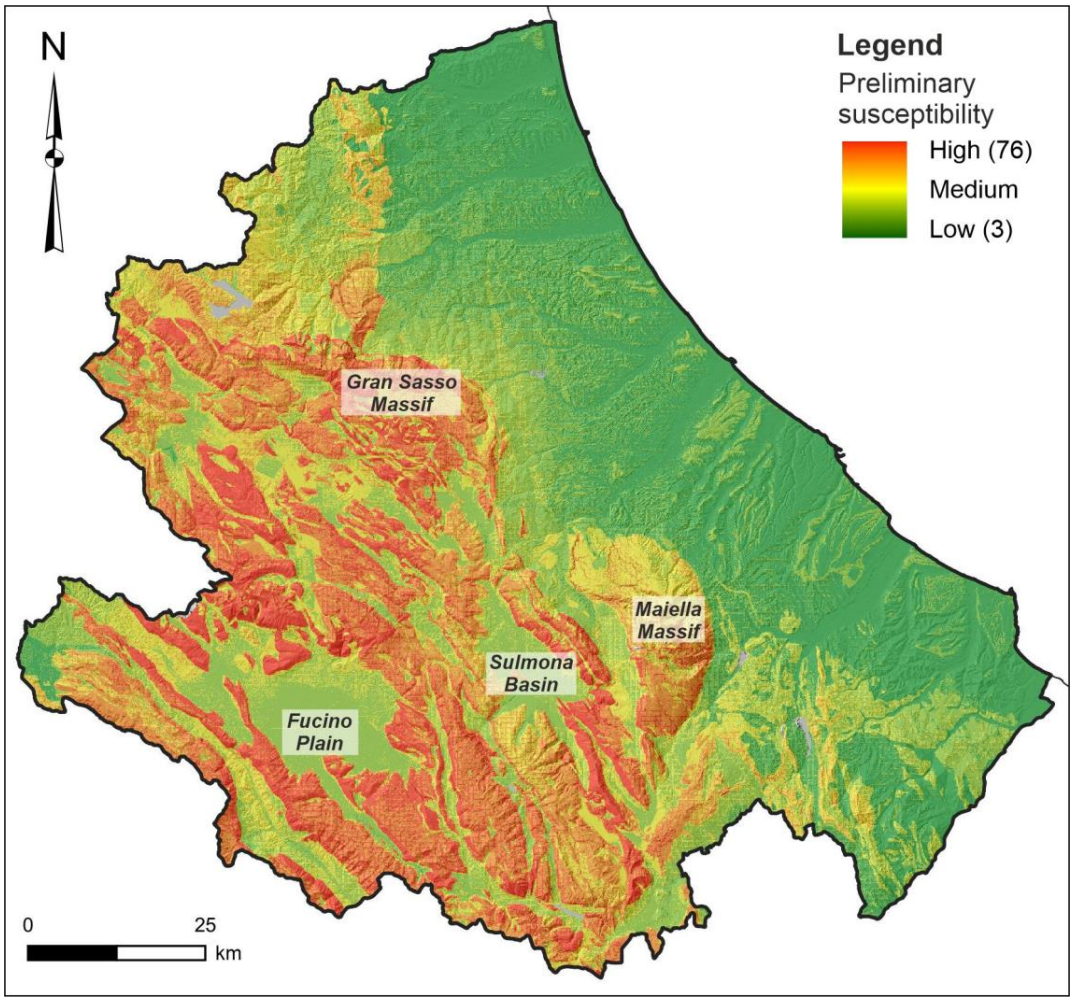

Figure 12. Preliminary susceptibility map.

4.3.2 Clusters determination, statistics, and susceptibility classes definition

The ratio between the total Within Clusters Sum of Squares (WCSS) and the Between Clusters Sum of Squares (BCSS) suddenly decreases, moving from 2 to 5 clusters and almost stabilises after this number. Accordingly, the related curve nearly flattens after this value, with a slope gradient progressively closer to zero (Figure 13).

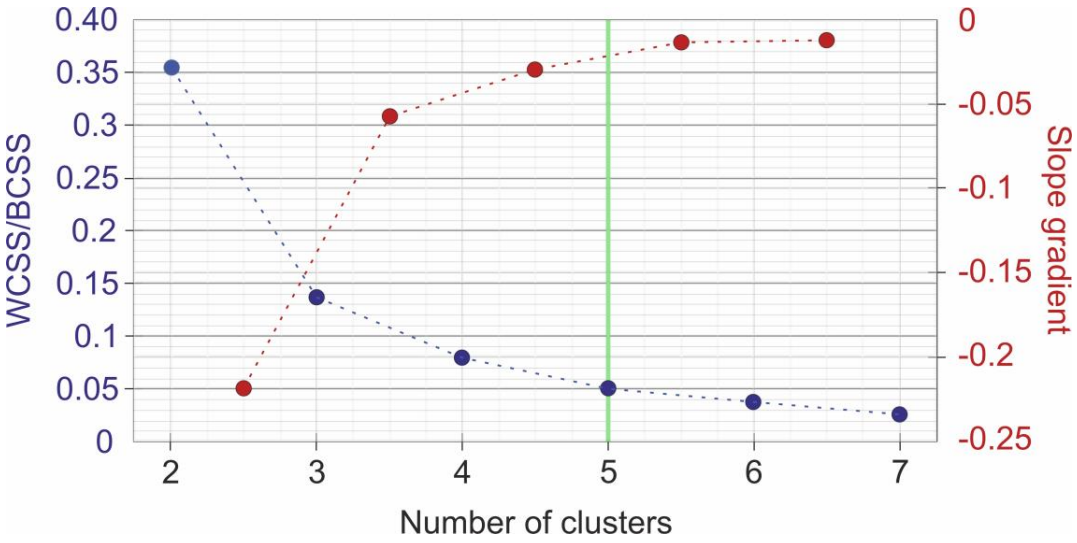

Figure 13. Plot of the WCSS/BCSS ratios (blue dotted line) against the number of clusters and related slope gradient (red dotted line). The solid green line indicates the optimal number of clusters identified through the elbow method.

From the above, five turns out to be the optimal number of clusters since an increase in this value does not result in a finer data clustering. Consequently, points of the Preliminary susceptibility raster are clustered into five groups.

From the analysis of values distribution within each cluster, it results that Cluster 3 contains the greatest volume of data, Cluster 5 the smallest one (Table 2); clusters 2 and 5 present, respectively, the narrowest and the widest extensions. Mean and median values are fairly near in each cluster; mode values slightly deviate from these. Cluster 2 shows the lowest standard deviation, while Cluster 5 the highest one. Finally, the InterQuartile Range (IQR) extensions of all clusters are rather comparable.

528 **Table 2.** Statistic of clusters.

Cluster #	Number of data-%	Values range	Mean-Median-Mode values	Standard deviation	IQR
1	22707492-21.2	3-16	12-12-12	2.64	10-14
2	23776539-22.1	17-25	21.1-21-24	2.62	19-24
3	25171384-23.4	26-36	30.4-30-26	3.15	28-33
4	20324367-18.9	37-47	42.2-42-47	3.16	39-45
5	15477554-14.4	48-76	52.6-52-48	3.83	49-55
Whole dataset	107457336-100	3-76	29.9-28-24	14.01	18-42

529

530 By comparing cluster statistics to classes of the absolute susceptibility scale of Figure 4 and by
531 applying the workflow of Figure 5, six susceptibility classes result ranging from I to VI out of VII
532 (Figure 14).

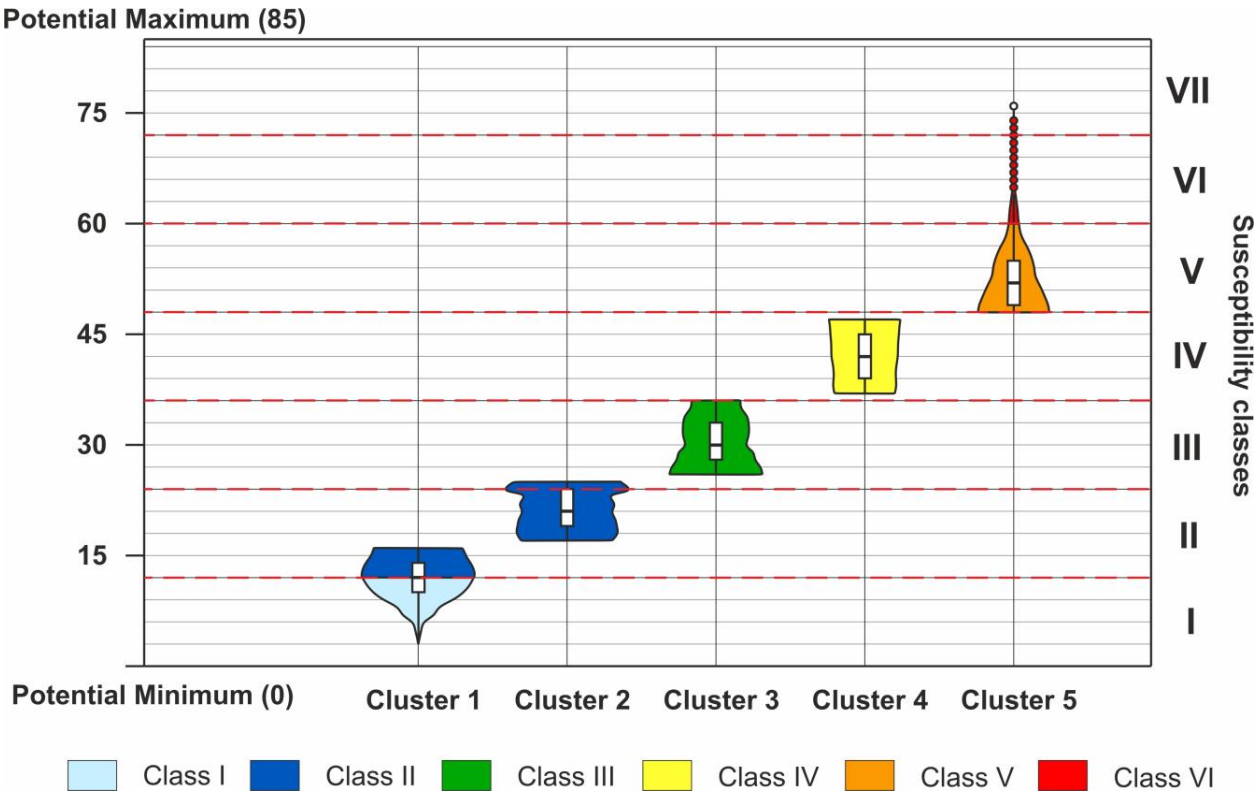

533

534 **Figure 14.** Violin plots of clusters data. Cluster 1 data greater than 12 constitute 35% of the group and are consequently
535 assigned to Class II. Cluster 5 data mostly fall into Class V but partially overcome the central value of the adjacent higher
536 class; consequently, values greater than 60 are assigned to Class VI. Concerning box-plots, lower and upper limits of

boxes represent the first (Q1) and the third (Q3) quartile of clusters data, lines inside the boxes the median values, whiskers the values greater than Q1 - 1.5·IQR and smaller than Q1 or greater than Q3 and smaller than Q3 + 1.5·IQR with IQR = Q3 - Q1. Circles represent the outliers, i.e., values smaller than Q1 - 1.5·IQR or greater than Q3 + 1.5·IQR.

4.3.3 Earthquake-induced landslides susceptibility map of the Abruzzo Region

The refinement of the susceptibility map results in the final detection of six susceptibility classes, ranging from I-Very Low to VI-High out of a maximum of VII (Figure 15).

Coastal areas are mostly characterised by Very Low susceptibility values. Low values are locally spotted in correspondence with high coasts and areas featuring the presence of anthropogenic sinkholes.

The piedmont area presents Very Low values, progressively increasing to Medium moving towards the chain sector. Fluvial plains are clearly distinguished from adjacent areas, having Very Low susceptibilities.

The chain sector, finally, presents values ranging from Medium-Low to High. In detail, the major intermontane basins (i.e., Fucino Plain and Sulmona Basin) are well described by Low and Medium-Low values; these last also characterise the northern portion of the Maiella massif. Medium and Medium-High susceptibilities are detected in correspondence of reliefs, moving to High values in correspondence of steep slopes, mostly on south-western flanks of ridges.

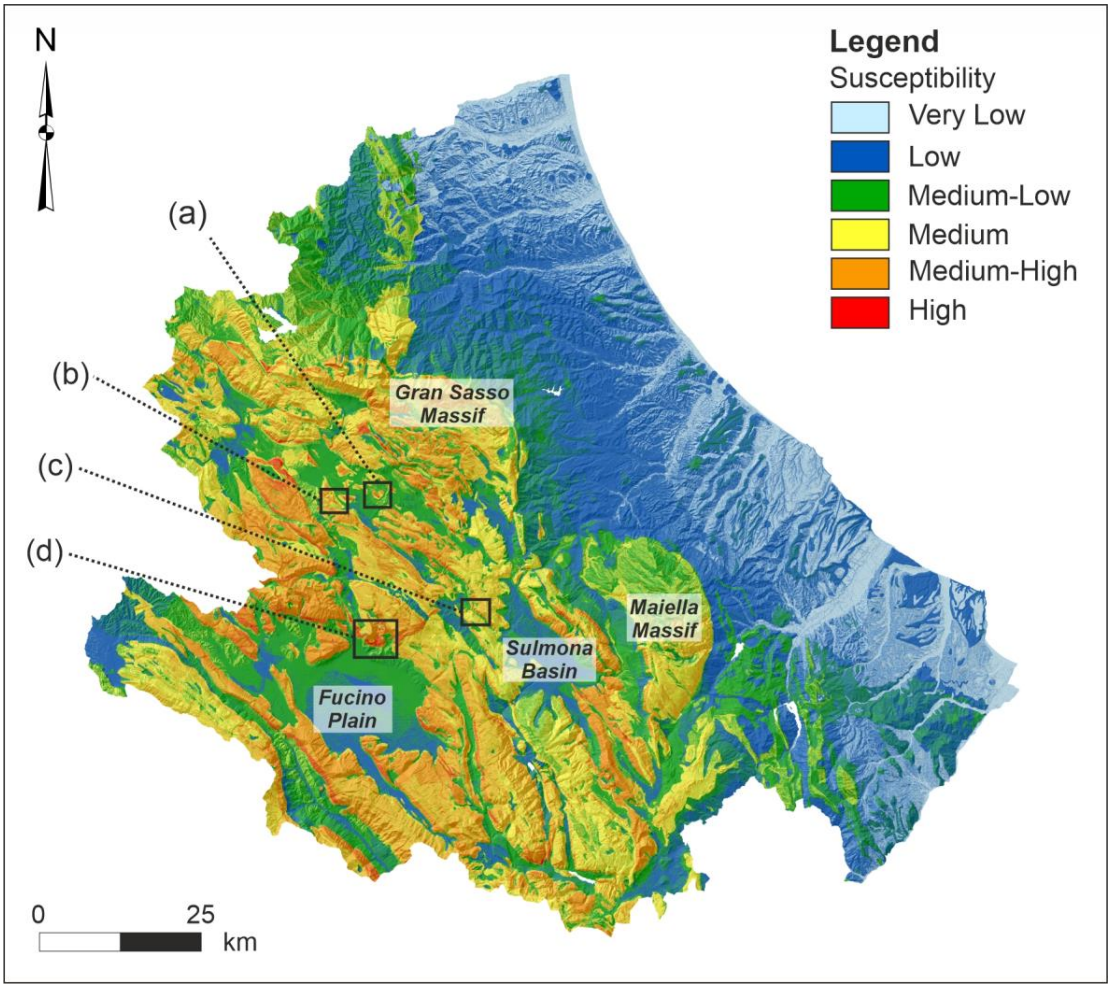

Figure 15. Earthquake-Induced Landslides (EILs) Susceptibility map of the Abruzzo Region. Black polygons indicate sectors presenting recorded EILs events; a detailed cartographic representation, supported by photo documentation, for each site is shown in Figure 16.

5. Discussions and conclusions

In this study, an expert-based approach followed by a statistical classification of resulting values is tested in order to evaluate the EILs susceptibility of the Abruzzo Region.

The comparison between sectors falling into different susceptibility classes and the geomorphological features of investigated areas highlight the quality of achieved results. The method, indeed, proves to be highly effective in distinguishing regions featuring different stability degrees, with well-known EILs detachments zones actually falling into Medium-High and High classes (Figure 16). Very Low to Medium values, on the other hand, mostly identify stable areas.

It is beyond question that the availability of good-quality data deeply affects the outcomes and that the accuracy of results increases as the number and the suitability of parameters increases. In this work, their choice and classification/weighting is performed by expert judgment, based on the critical analysis of literature data as well as of inventoried landslide events; the combination of nine morphometric and geothematic features turns out to be highly proper.

In the case of parameters affecting limited sectors of the study area and here referred to as secondary ones, it is advisable not to consider their contribution in the definition of the minimum/maximum potential values in order to avoid the relative scale compaction with respect to the absolute one and the subsequent lowering of detected susceptibility degrees. Their impact is to be assessed in a second phase. The question is here managed by excluding the *Anthropogenic sinkholes* factor in the heuristic analysis to later sum their associated weight to the Susceptibility map right before the final classification step.

The analysis of variance performed on clusters resulting from Forgy's Kmeans algorithm allows the detection of the most suitable number of data groups actually present in the study area. Nevertheless, a statistical analysis of these data groups is required, given their variable extension, in order to assign them the appropriate susceptibility class. A correction of limits detected through the process is opportune and desirable in cases of clustered values encompassing too wide ranges or a relevant percentage of data falling into a class different from the most populated one. The workflow presented in this paper proves to be highly effective in this regard.

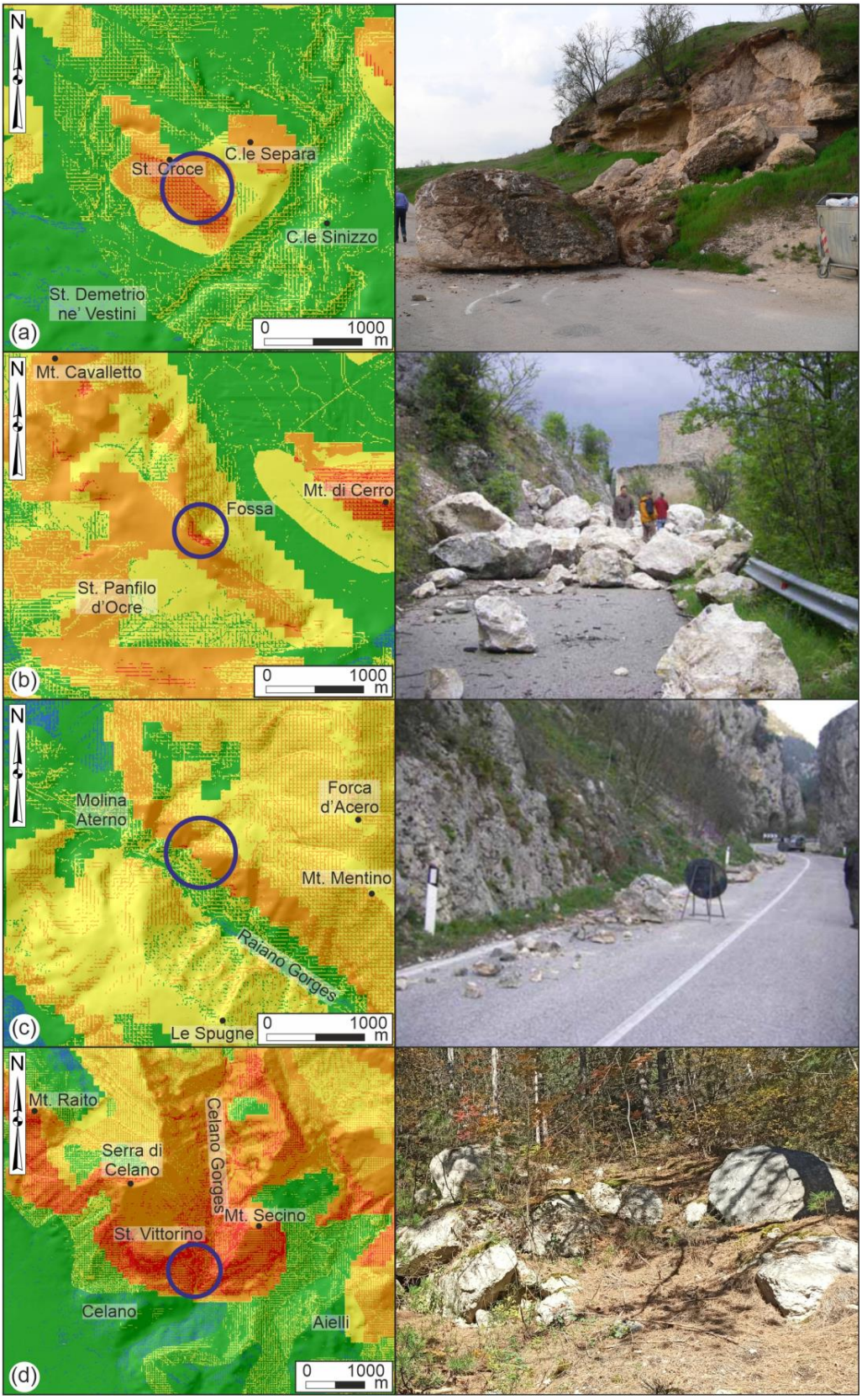

586

587 **Figure 16.** Photo documentation of recorded EILs events over Abruzzo Region; for site locations and legend, see Figure

588 15. On the left, magnification the resulting landslide susceptibility map (Figure 15) for each site: a) San Demetrio ne'

589 Vestini (AQ), b) Fossa (AQ), c) Raiano (AQ), d) Celano (AQ); on the right, photo documentation of selected EILs events
590 (Figure 16b and c are modified from Blumetti et al., 2009). Blue circles indicate detachments areas.

591 In conclusion, an accurate EILs susceptibility evaluation of the Abruzzo region is achieved by joining
592 expert-based heuristic and statistical analyses. Results here presented highlight the robustness of the
593 approach; remarkably, the applied methodology overcomes limits eventually intrinsic to catalogues,
594 making the approach a valuable tool in the development of territorial planning, emergency
595 management, and loss-reduction measures, readily applicable even in areas where fairly detailed EILs
596 data are missing. The statistical analyses and the adoption of an absolute scale ranging from minimum
597 to maximum potential values, finally, ensures the comparability of results among different study
598 areas, if the same classification and weighting of parameters here used are applied.

599 **Funding:** This work was supported by the Project "*Integrated and multi-scale approach for the*
600 *definition of earthquake-induced landslide hazard in the Italian territory*" funded by the Italian
601 Ministry of Environment, Land and Sea.

602 **Acknowledgements:** The authors thank the Cartographic Office of the Abruzzo Region for the
603 material available at the Open Geodata Portal (http://opendata.regione.abruzzo.it/) and the Italian
604 Ministry of Environment, Land and Sea (http://www.minambiente.it/) for providing topographic data
605 and Digital Elevation Model (DEM) used in this study.

606 **References**

607 Abruzzo Region, 2011. Primo progetto di variante del Piano Stralcio di bacino per l'Assetto
608 Idrogeologico - "Fenomeni gravitativi e processi erosivi" dei bacini di rilievo regionale
609 dell'Abruzzo e del bacino interregionale del fiume Sangro. L'Aquila, Italy.

610 Abruzzo Region, 2019. Approvazione della I variante parziale del Piano stralcio di bacino per
611 l'Assetto Idrogeologico - "Fenomeni gravitati e processi erosivi", riferito ai bacini di rilievo

612 regionale dell'Abruzzo e al territorio regionale ricompreso nel bacino interregionale. L'Aquila,
613 Italy.

614 Accordi, B., Carbone, F., 1988. Carta delle litofacies del Lazio-Abruzzi ed aree limitrofe. Quad. Ric.
615 Sci. 114

616 Aleotti, P., Chowdhury, R., 1999. Landslide hazard assessment: Summary review and new
617 perspectives. Bull. Eng. Geol. Environ. 58, 21-44. https://doi.org/10.1007/s100640050066

618 Amato, G., Fiorucci, M., Martino, S., Lombardo, L., Palombi, L., 2021. Earthquake-triggered
619 landslide susceptibility in Italyby means of Artificial Neural Network. Earth ArXiv. Preprint.
620 https://doi.org/10.31223/X59W39

621 Ascione, A., Cinque, A., Miccadei, E., Villani, F., Berti, C., 2008. The Plio-Quaternary uplift of the
622 Apennine chain: new data from the analysis of topography and river valleys in Central Italy.
623 Geomorphology 102, 105-118. https://doi.org/10.1016/j.geomorph.2007.07.022

624 Baratta, M., 1901. I terremoti d'Italia. Saggio di storia, geografia e bibliografia sismica italiana.
625 Torino, Italy.

626 Barisone, G., Bottino, G., Mandrone, G., 1994. Correlations among geomechanical characteristics,
627 fracturation degree and stability of rock slopes. Int. J. Rock Mech. Min. Sci. Geomech. Abstr.
628 31, A108. https://doi.org/10.1016/0148-9062(94)93183-6

629 Basili, R., Valensise, G., Vannoli, P., Burrato, P., Fracassi, U., Mariano, S., Tiberti, M.M., Boschi,
630 E., 2008. The Database of Individual Seismogenic Sources (DISS), version 3: Summarising 20
631 years of research on Italy's earthquake geology. Tectonophysics 453, 20-43.
632 https://doi.org/10.1016/j.tecto.2007.04.014

633 Bigi, S., Cantalamessa, G., Centamore, E., Didaskalou, P., Dramis, F., Farabollini, P., Gentili, B.,
634 Nvernizzi, C., Micarelli, A., Nisio, S., Pambianchi, G., Potetti, M., 1995. La fascia periadriatica
635 marchigiano-abruzzese dal pliocene medio ai tempi attuale: evoluzione tettonico-sedimentaria e
636 geomorfologica. Stud. Geol. Camerti Vol. Spec., 37-49. https://doi.org/10.15165/studgeocam-
637 886

638 Bigi, S., Conti, A., Casero, P., Ruggiero, L., Recanati, R., Lipparini, L., 2013. Geological model of
639 the central Periadriatic basin (Apennines, Italy). Mar. Pet. Geol. 42, 107-121.
640 https://doi.org/10.1016/j.marpetgeo.2012.07.005

641 Blumetti, A.M., Comerci, V., Di Manna, P., Guerrieri, L., Vittori, E., 2009. Geological effects
642 induced by the L'Aquila earthquake (6 April 2009, Ml = 5.8) on the natural environment -
643 Preliminary report, Environment. Rome, Italy.

644 Boncio, P., Lavecchia, G., Pace, B., 2004. Defining a model of 3D seismogenic sources for Seismic
645 Hazard Assessment applications: The case of central Apennines (Italy). J. Seismol. 8, 407-425.
646 https://doi.org/10.1023/B:JOSE.0000038449.78801.05

647 Boncio, P., Tinari, D.P., Lavecchia, G., Visini, F., Milana, G., 2009. The instrumental seismicity of
648 the Abruzzo Region in Central Italy (1981-2003): seismotectonic implications. Boll. della Soc.
649 Geol. Ital. 128, 367-380. https://doi.org/10.3301/IJG.2009.128.2.367

650 Bozzano, F., Mazzanti, P., Prestininzi, A., Mugnozza, G.S., 2010. Research and development of
651 advanced technologies for landslide hazard analysis in Italy. Landslides 7, 381-385.
652 https://doi.org/10.1007/s10346-010-0208-x

653 Calista, M., Mascioli, F., Menna, V., Miccadei, E., Piacentini, T., 2019. Recent geomorphological
654 evolution and 3d numerical modelling of soft clastic rock cliffs in the mid-western adriatic sea
655 (Abruzzo, italy). Geosci. 9, 309. https://doi.org/10.3390/geosciences9070309

Calista, M., Menna, V., Mancinelli, V., Sciarra, N., Miccadei, E., 2020. Rockfall and Debris Flow Hazard Assessment in the SW Escarpment of Montagna del Morrone Ridge (Abruzzo, Central Italy). Water (Switzerland) 12, 1206. https://doi.org/10.3390/w12041206

Capitani, M., Ribolini, A., Bini, M., 2013. The slope aspect: A predisposing factor for landsliding? Comptes Rendus - Geosci. 345, 427-438. https://doi.org/10.1016/j.crte.2013.11.002

Caprari, P., Della Seta, M., Martino, S., Fantini, A., Fiorucci, M., Priore, T., 2018. Upgrade of the CEDIT database of earthquake-induced ground effects in Italy. Ital. J. Eng. Geol. Environ. 2, 23–39. https://doi.org/10.4408/IJEGE.2018-02.O-02

Carabella, C., Boccabella, F., Buccolini, M., Ferrante, S., Pacione, A., Gregori, C., Pagliani, T., Piacentini, T., Miccadei, E., 2021. Geomorphology of landslide–flood-critical areas in hilly catchments and urban areas for EWS (Feltrino Stream and Lanciano town, Abruzzo, Central Italy). J. Maps 17, 40–53. https://doi.org/10.1080/17445647.2020.1819903

Carabella, C., Miccadei, E., Paglia, G., Sciarra, N., 2019. Post-Wildfire Landslide Hazard Assessment: The Case of The 2017 Montagna Del Morrone Fire (Central Apennines, Italy). Geosciences 9, 175. https://doi.org/10.3390/geosciences9040175

Carafa, M.M.C., Galvani, A., Di Naccio, D., Kastelic, V., Di Lorenzo, C., Miccolis, S., Sepe, V., Pietrantonio, G., Gizzi, C., Massucci, A., Valensise, G., Bird, P., 2020. Partitioning the Ongoing Extension of the Central Apennines (Italy): Fault Slip Rates and Bulk Deformation Rates From Geodetic and Stress Data. J. Geophys. Res. Solid Earth 125, e2019JB018956. https://doi.org/10.1029/2019JB018956

Carrara, A., Cardinali, M., Detti, R., Guzzetti, F., Pasqui, V., Reichenbach, P., 1991. GIS techniques and statistical models in evaluating landslide hazard. Earth Surf. Process. Landforms 16, 427-445. https://doi.org/10.1002/esp.3290160505

679 Cascini, L., 2008. Applicability of landslide susceptibility and hazard zoning at different scales. Eng.
680 Geol. 102, 164-177. https://doi.org/10.1016/j.enggeo.2008.03.016

681 Çevik, E., Topal, T., 2003. GIS-based landslide susceptibility mapping for a problematic segment of
682 the natural gas pipeline, Hendek (Turkey). Environ. Geol. 44, 949-962.
683 https://doi.org/10.1007/s00254-003-0838-6

684 Chigira, M., Yagi, H., 2006. Geological and geomorphological characteristics of landslides triggered
685 by the 2004 Mid Niigta prefecture earthquake in Japan. Eng. Geol. 82, 202–221.
686 https://doi.org/10.1016/j.enggeo.2005.10.006

687 Crescenti, U., Dramis, F., Gentili, B., Praturlon, A., 1984. The Bisaccia landslide: a case of deep-
688 seated gravitational movement reactivated by earthquakes. Proc. Coll. “Mouvements de Terrain”
689 83, 15-21.

690 D’Agostino, N., Jackson, J.A., Dramis, F., Funiciello, R., 2001. Interactions between mantle
691 upwelling, drainage evolution and active normal faulting: An example from the Central
692 Appennines (Italy). Geophys. J. Int. 147, 475-497. https://doi.org/10.1046/j.1365-
693 246X.2001.00539.x

694 D’Alessandro, L., Miccadei, E., Piacentini, T., 2003. Morphostructural elements of central-eastern
695 Abruzzi: Contributions to the study of the role of tectonics on the morphogenesis of the
696 Apennine chain. Quat. Int. 101-102, 115-124. https://doi.org/10.1016/S1040-6182(02)00094-0

697 D’Alessandro, L., Miccadei, E., Piacentini, T., 2008. Morphotectonic study of the lower Sangro River
698 valley (Abruzzi, Central Italy). Geomorphology 102, 145-158.
699 https://doi.org/10.1016/j.geomorph.2007.06.019

Della Seta, M., Del Monte, M., Fredi, P., Miccadei, E., Nesci, O., Pambianchi, G., Piacentini, T., Troiani, F., 2008. Morphotectonic evolution of the Adriatic piedmont of the Apennines: An advancement in the knowledge of the Marche-Abruzzo border area. Geomorphology 102, 119-129. https://doi.org/10.1016/j.geomorph.2007.06.018

Demangeot, J., 1965. Géomorphologie des Abruzzes Adriatiques. Centre Rechèrche et Documentation Cartographiques Memories et Documents, Paris, France.

Di Bucci, D., Angeloni, P., 2013. Adria seismicity and seismotectonics: Review and critical discussion. Mar. Pet. Geol. 42, 182-190. https://doi.org/10.1016/j.marpetgeo.2012.09.005

DISS Working Group, 2018. Database of Individual Seismogenic Sources (DISS), Version 3.2.1: A compilation of potential sources for earthquakes larger than M 5.5 in Italy and surrounding areas. http://diss.rm.ingv.it/diss/, Istituto Nazionale di Geofisica e Vulcanologia. https://doi.org/10.6092/INGV.IT-DISS3.2.1.

EMERGEO Working Group, Pucci, S., De Martini, P.M., Civico, R., Nappi, R., Ricci, T., Villani, F., Brunori, C.A., Caciagli, M., Sapia, V., Cinti, F.R., Moro, M., Di Naccio, D., Gori, S., Falcucci, E., Vallone, R., Mazzarini, F., Tarquini, S., Del Carlo, P., Kastelic, V., Carafa, M., De Ritis, R., Gaudiosi, G., Nave, R., Alessio, G., Burrato, P., Smedile, A., Alfonsi, L., Vannoli, P., Pignone, M., Pinzi, S., Fracassi, U., Pizzimenti, L., Mariucci, M.T., Pagliuca, N., Sciarra, A., Carluccio, R., Nicolosi, I., Chiappini, M., D'Ajello Caracciolo, F., Pezzo, G., Patera, A., Azzaro, R., Pantosti, D., Montone, P., Saroli, M., Lo Sardo, L., Lancia, M., 2016. Coseismic effects of the 2016 Amatrice seismic sequence: First geological results. Ann. Geophys. 59. https://doi.org/10.4401/ag-7195

Esposito, G., Carabella, C., Paglia, G., Miccadei, E., 2021. Relationships between Morphostructural/Geological Framework and Landslide Types: Historical Landslides in the

723 Hilly Piedmont Area of Abruzzo Region (Central Italy). Land 10, 287.
724 https://doi.org/10.3390/land10030287

725 Fan, X., Scaringi, G., Korup, O., West, A.J., van Westen, C.J., Tanyas, H., Hovius, N., Hales, T.C.,
726 Jibson, R.W., Allstadt, K.E., Zhang, L., Evans, S.G., Xu, C., Li, G., Pei, X., Xu, Q., Huang, R.,
727 2019. Earthquake-Induced Chains of Geologic Hazards: Patterns, Mechanisms, and Impacts.
728 Rev. Geophys. 57, 421-503. https://doi.org/10.1029/2018RG000626

729 Fell, R., Whitt, G., Miner, T., Flentje, P., 2008. Guidelines for landslide susceptibility, hazard and
730 risk zoning for land use planning. Eng. Geol. 102, 83-84.
731 https://doi.org/10.1016/j.enggeo.2008.03.009

732 Fiore, A., Lanzini, M., 2007. Problematiche di valutazione del rischio di crollo di cavità sotterranee.
733 Geol. Territ. 1, 35-45.

734 Forgy, E., 1965. Cluster analysis of multivariate data: Efficiency vs. interpretability of classification.
735 Biometrics 21, 768-769.

736 Fortunato, C., Martino, S., Prestininzi, A., Romeo, R.W., 2012. New release of the italian catalogue
737 of earthquake-induced ground failures (CEDIT). Ital. J. Eng. Geol. Environ. 2, 63-74.
738 https://doi.org/DOI: 10.4408/IJEGE.2012-02.O-05

739 Fracassi, U., Valensise, G., 2007. Unveiling the sources of the catastrophic 1456 multiple earthquake:
740 Hints to an unexplored tectonic mechanism in southern Italy. Bull. Seismol. Soc. Am. 97, 725-
741 748. https://doi.org/10.1785/0120050250

742 Gorini, A., Marcucci, S., Marsan, P., Milana, G., 2004. Strong motion records of the 2002 Molise,
743 Italy, earthquake sequence and stochastic simulation of the main shock. Earthq. Spectra 20, 65-
744 79. https://doi.org/10.1193/1.1764784

745 Guerrieri, L., 2015. Earthquake Environmental Effect for seismic hazard assessment: the ESI
746 intensity scale and the EEE Catalogue. Mem. Descr. della Cart. Geol. d'Italia 97.

747 Guidoboni, E., Ferrari, G., Tarabusi, G., Sgattoni, G., Comastri, A., Mariotti, D., Ciuccarelli, C.,
748 Bianchi, M.G., Valensise, G., 2019. CFTI5Med, the new release of the catalogue of strong
749 earthquakes in Italy and in the Mediterranean area. Sci. Data 6, 80.
750 https://doi.org/10.1038/s41597-019-0091-9

751 Guzzetti, F., Carrara, A., Cardinali, M., Reichenbach, P., 1999. Landslide hazard evaluation: A
752 review of current techniques and their application in a multi-scale study, Central Italy.
753 Geomorphology 31, 181-216. https://doi.org/10.1016/S0169-555X(99)00078-1

754 Guzzetti, F., Reichenbach, P., Ardizzone, F., Cardinali, M., Galli, M., 2006. Estimating the quality
755 of landslide susceptibility models. Geomorphology 81, 166-184.
756 https://doi.org/10.1016/j.geomorph.2006.04.007

757 Guzzetti, F., Reichenbach, P., Cardinali, M., Galli, M., Ardizzone, F., 2005. Probabilistic landslide
758 hazard assessment at the basin scale. Geomorphology 72, 272-299.
759 https://doi.org/10.1016/j.geomorph.2005.06.002

760 Hasegawa, S., Dahal, R.K., Nishimura, T., Nonomura, A., Yamanaka, M., 2009. DEM-Based
761 analysis of earthquake-induced shallow landslide susceptibility. Geotech. Geol. Eng. 27, 419-
762 430. https://doi.org/10.1007/s10706-008-9242-z

763 ISIDe Working Group, 2007. Italian Seismological Instrumental and Parametric Database (ISIDe).
764 Istituto Nazionale di Geofisica e Vulcanologia. https://doi.org/10.13127/ISIDE

765 ISPRA, 2007. Inventarion dei Fenomeni Franosi in Italia - IFFI - Regione Abruzzo.

766 ISPRA, 2017. The Geological map of Italy 1:50,000 scale - The CARG project. Mem. Descr. della
767 Cart. Geol. d'Italia 100, 127-198.

768 ISPRA, 2020. Database Nazionale Sinkhole [WWW Document]. URL
769 http://sgi.isprambiente.it/sinkholeweb/ (accessed 9.25.20).

770 ISRM, 1978. Suggested methods for the quantitative description of discontinuities in rock masses.
771 Int. J. Rock Mech. Min. Sci. Geomech. Abstr. 15, 319-368. https://doi.org/10.1016/0148-
772 9062(79)91476-1

773 ITHACA Working Group, 2019. ITHACA (ITaly HAzard from CApable faulting), A database of
774 active capable faults of the Italian territory. Version December 2019. ISPRA Geological Survey
775 of Italy. Web Portal http://sgi2.isprambiente.it/ithacaweb/Mappatura.aspx

776 Kastelic, V., Vannoli, P., Burrato, P., Fracassi, U., Tiberti, M.M., Valensise, G., 2013. Seismogenic
777 sources in the Adriatic Domain. Mar. Pet. Geol. 42, 191-213.
778 https://doi.org/10.1016/j.marpetgeo.2012.08.002

779 Keefer, D.K., 1984. Landslide caused by earthquakes. Bull. Geol. Soc. Am. 95, 406-421.
780 https://doi.org/10.1130/0016-7606(1984)95<406:lcbe>2.0.co;2

781 Keefer, D.K., 2002. Investigating landslides caused by earthquakes - A historical review. Surv.
782 Geophys. 23, 473-510. https://doi.org/10.1023/A:1021274710840

783 Komac, M., 2006. A landslide susceptibility model using the Analytical Hierarchy Process method
784 and multivariate statistics in perialpine Slovenia. Geomorphology 74, 17-28.
785 https://doi.org/10.1016/j.geomorph.2005.07.005

786 Konovalov, A., Gensiorovskiy, Y., Lobkina, V., Muzychenko, A., Stepnova, Y., Muzychenko, L.,
787 Stepnov, A., Mikhalyov, M., 2019. Earthquake-induced landslide risk assessment: An example
788 from Sakhalin Island, Russia. Geosci. 9, 305. https://doi.org/10.3390/geosciences9070305

789 Livio, F., Ferrario, M.F., 2020. Assessment of attenuation regressions for earthquake-triggered
790 landslides in the Italian Apennines: insights from recent and historical events. Landslides 17,
791 2825-2836. https://doi.org/10.1007/s10346-020-01464-w

792 Luzi, L., Pacor, F., Puglia, R., Lanzano, G., Felicetta, C., D'Amico, M., Michelini, A., Faenza, L.,
793 Lauciani, V., Iervolino, I., Baltzopoulos, G., Chioccarelli, E., 2017. The central Italy seismic
794 sequence between August and December 2016: Analysis of strong-motion observations.
795 Seismol. Res. Lett. 88, 1219-1231. https://doi.org/10.1785/0220170037

796 Magliulo, P., Di Lisio, A., Russo, F., 2009. Comparison of GIS-based methodologies for the landslide
797 susceptibility assessment. Geoinformatica 13, 253-265. https://doi.org/10.1007/s10707-008-
798 0063-2

799 Marchesini, I., Ardizzone, F., Alvioli, M., Rossi, M., Guzzetti, F., 2014. Non-susceptible landslide
800 areas in Italy and in the Mediterranean region. Nat. Hazards Earth Syst. Sci. 14, 2215-2231.
801 https://doi.org/10.5194/nhess-14-2215-2014

802 Marsala, V., Galli, A., Paglia, G., Miccadei, E., 2019. Landslide susceptibility assessment of
803 Mauritius Island (Indian ocean). Geosci. 9, 493. https://doi.org/10.3390/geosciences9120493

804 Martino, S., Antonielli, B., Bozzano, F., Caprari, P., Discenza, M.E., Esposito, C., Fiorucci, M.,
805 Iannucci, R., Marmoni, G.M., Schilirò, L., 2020. Landslides triggered after the 16 August 2018
806 Mw 5.1 Molise earthquake (Italy) by a combination of intense rainfalls and seismic shaking.
807 Landslides 17, 1177-1190. https://doi.org/10.1007/s10346-020-01359-w

808 Martino, S., Bozzano, F., Caporossi, P., D'Angiò, D., Della Seta, M., Esposito, C., Fantini, A.,
809 Fiorucci, M., Giannini, L.M., Iannucci, R., Marmoni, G.M., Mazzanti, P., Missori, C., Moretto,
810 S., Piacentini, D., Rivellino, S., Romeo, R.W., Sarandrea, P., Schilirò, L., Troiani, F., Varone,
811 C., 2019. Impact of landslides on transportation routes during the 2016–2017 Central Italy
812 seismic sequence. Landslides 16, 1221–1241. https://doi.org/10.1007/s10346-019-01162-2

813 Martino, S., Prestininzi, A., Romeo, R.W., 2014. Earthquake-induced ground failures in Italy from a
814 reviewed database. Nat. Hazards Earth Syst. Sci. 14, 799-814. https://doi.org/10.5194/nhess-14-
815 799-2014

816 Mascioli, F., Piattelli, V., Cerrone, F., Gasprino, D., Kunde, T., Miccadei, E., 2021. Feasibility of
817 Objective Seabed Mapping Techniques in a Coastal Tidal Environment (Wadden Sea,
818 Germany). Geosci. 11, 49. https://doi.org/10.3390/geosciences11020049

819 Maufroy, E., Lacroix, P., Chaljub, E., Sira, C., Grelle, G., Bonito, L., Causse, M., Cruz-Atienza,
820 V.M., Hollender, F., Cotton, F., Bard, P.-Y., 2018. Towards rapid prediction of topographic
821 amplification at small scales : contribution of the FSC proxy and pleiades terrain models for the
822 2016 Amatrice earthquake (Italy, MW 6.0)., in: 16th European Conference on Earthquake
823 Engineering. 18-21 June, Thessaloniki, Greece.

824 Miccadei, E., Carabella, C., Paglia, G., Piacentini, T., 2018. Paleo-drainage network,
825 morphotectonics, and fluvial terraces: Clues from the verde stream in the middle Sangro river
826 (central italy). Geosci. 8, 337. https://doi.org/10.3390/geosciences8090337

827 Miccadei, E., Mascioli, F., Ricci, F., Piacentini, T., 2019. Geomorphology of soft clastic rock coasts
828 in the mid-western Adriatic Sea (Abruzzo, Italy). Geomorphology 324, 72-94.
829 https://doi.org/10.1016/j.geomorph.2018.09.023

Miccadei, E., Piacentini, T., Buccolini, M., 2017. Long-term geomorphological evolution in the Abruzzo area, Central Italy: Twenty years of research. Geol. Carpathica 68, 19-28. https://doi.org/10.1515/geoca-2017-0002

Miccadei, E., Piacentini, T., Gerbasi, F., Daverio, F., 2012. Morphotectonic map of the Osento River basin (Abruzzo, Italy), scale 1:30,000. J. Maps 8, 62-73. https://doi.org/10.1080/17445647.2012.668764

Miccadei, E., Piacentini, T., Sciarra, N., 2010. Landslides seismically induced during the earthquake of 6 April 2009 in Abruzzo Region (Central Italy), in: Geologically Active - Proceedings of the 11th IAEG Congress. Auckland, New Zealand, pp. 127-141.

Michetti, A.M., Serva, L., Vittori, E., 2000. ITHACA Italy Hazard from Capable Faults: a database of active faults of the Italian onshore territory.

Molnar, P., Anderson, R.S., Anderson, S.P., 2007. Tectonics, fracturing of rock, and erosion. J. Geophys. Res. Earth Surf. 112. https://doi.org/10.1029/2005JF000433

Nisio, S., Caramanna, G., Ciotoli, G., 2007. Sinkholes in Italy: First results on the inventory and analysis. Geol. Soc. Spec. Publ. 279, 23-45. https://doi.org/10.1144/SP279.4

Nowicki Jessee, M.A., Hamburger, M.W., Ferrara, M.R., McLean, A., FitzGerald, C., 2020. A global dataset and model of earthquake-induced landslide fatalities. Landslides 17, 1363-1376. https://doi.org/10.1007/s10346-020-01356-z

Oswald, P., Strasser, M., Hammerl, C., Moernaut, J., 2021. Seismic control of large prehistoric rockslides in the Eastern Alps. Nat. Commun. 12, 1059. https://doi.org/10.1038/s41467-021-21327-9

851 Pace, B., Valentini, A., Ferranti, L., Vasta, M., Vassallo, M., Montagna, P., Colella, A., Pons-
852 Branchu, E., 2020. A Large Paleoearthquake in the Central Apennines, Italy, Recorded by the
853 Collapse of a Cave Speleothem. Tectonics 29. https://doi.org/10.1029/2020TC006289

854 Parotto, M., Cavinato, G.P., Miccadei, E., Tozzi, M., 2004. Line CROP 11: Central Apennines, in:
855 Scrocca, D., Doglioni, C., Innocenti, F., Manetti, P., Mazzotti, A., Bertelli, L., Burbi, L.,
856 D'Offizi, S. (Eds.), CROP Atlas: Seismic Reflection Profiles of the Italian Crust. Memorie
857 Descrittive della Carta Geologica d'Italia, Rome, Italy, pp. 145-153.

858 Pasculli, A., Palermi, S., Sarra, A., Piacentini, T., Miccadei, E., 2014. A modelling methodology for
859 the analysis of radon potential based on environmental geology and geographically weighted
860 regression. Environ. Model. Softw. 54, 165-181. https://doi.org/10.1016/j.envsoft.2014.01.006

861 Patacca, E., Scandone, P., Di Luzio, E., Cavinato, G.P., Parotto, M., 2008. Structural architecture of
862 the central Apennines: Interpretation of the CROP 11 seismic profile from the Adriatic coast to
863 the orographic divide. Tectonics 27, TC3006. https://doi.org/10.1029/2005TC001917

864 Petley, D., 2012. Global patterns of loss of life from landslides. Geology 40, 927-930.
865 https://doi.org/10.1130/G33217.1

866 Pham, B.T., Tien Bui, D., Pourghasemi, H.R., Indra, P., Dholakia, M.B., 2017. Landslide
867 susceptibility assesssment in the Uttarakhand area (India) using GIS: a comparison study of
868 prediction capability of naïve bayes, multilayer perceptron neural networks, and functional trees
869 methods. Theor. Appl. Climatol. 128, 255-273. https://doi.org/10.1007/s00704-015-1702-9

870 Piacentini, T., Calista, M., Crescenti, U., Miccadei, E., Sciarra, N., 2020. Seismically induced snow
871 avalanches: The central Italy case. Front. Earth Sci. 8, 1-27.
872 https://doi.org/10.3389/feart.2020.599611

873 Piacentini, T., Miccadei, E., 2014. The role of drainage systems and intermontane basins in the
874 Quaternary landscape of the Central Apennines chain (Italy). Rend. Lincei 25, 139-150.
875 https://doi.org/10.1007/s12210-014-0312-2

876 Piacentini, T., Miccadei, E., Di Michele, R., Sciarra, N., Mataloni, G., 2013. Geomorphological
877 analysis applied to rock falls in Italy: The case of the san venanzio gorges (Aterno river,
878 Abruzzo, Italy). Ital. J. Eng. Geol. Environ. 467-479.

879 Pischiutta, M., Fondriest, M., Demurtas, M., Magnoni, F., Di Toro, G., Rovelli, A., 2017. Structural
880 control on the directional amplification of seismic noise (Campo Imperatore, central Italy). Earth
881 Planet. Sci. Lett. 471, 10-18. https://doi.org/10.1016/j.epsl.2017.04.017

882 Pourghasemi, H.R., Teimoori Yansari, Z., Panagos, P., Pradhan, B., 2018. Analysis and evaluation
883 of landslide susceptibility: a review on articles published during 2005-2016 (periods of 2005-
884 2012 and 2013-2016). Arab. J. Geosci. 11, 193. https://doi.org/10.1007/s12517-018-3531-5

885 Rapolla, A., Di Nocera, S., Matano, F., Paoletti, V., Tarallo, D., 2012. Susceptibility regional zonation
886 of earthquake-induced landslides in Campania, Southern Italy. Nat. Hazards 61, 115-126.
887 https://doi.org/10.1007/s11069-011-9790-z

888 Reichenbach, P., Rossi, M., Malamud, B.D., Mihir, M., Guzzetti, F., 2018. A review of statistically-
889 based landslide susceptibility models. Earth-Science Rev. 180, 60-91.
890 https://doi.org/10.1016/j.earscirev.2018.03.001

891 Rovida, A., Locati, M., Camassi, R., Lolli, B., Gasperini, P., Antonucci, A., 2021. The Italian
892 earthquake catalogue CPTI15 - Version 3.0. Istituto Nazionale di Geofisica e Vulcanologia.
893 https://doi.org/10.13127/CPTI/CPTI15.3

Ruff, M., Czurda, K., 2008. Landslide susceptibility analysis with a heuristic approach in the Eastern Alps (Vorarlberg, Austria). Geomorphology 94, 314-324. https://doi.org/10.1016/j.geomorph.2006.10.032

Salvati, P., Bianchi, C., Rossi, M., Guzzetti, F., 2010. Societal landslide and flood risk in Italy. Nat. Hazards Earth Syst. Sci. 10, 465-483. https://doi.org/10.5194/nhess-10-465-2010

Santo, A., Del Prete, S., Di Crescenzo, G., Rotella, M., 2007. Karst processes and slope instability: Some investigations in the carbonate Apennine of Campania (southern Italy). Geol. Soc. Spec. Publ. 279, 59-72. https://doi.org/10.1144/SP279.6

Sembroni, A., Molin, P., Soligo, M., Tuccimei, P., Anzalone, E., Billi, A., Franchini, S., Ranaldi, M., Tarchini, L., 2020. The uplift of the Adriatic flank of the Apennines since the Middle Pleistocene: New insights from the Tronto River basin and the Acquasanta Terme Travertine (central Italy). Geomorphology 352, 106990. https://doi.org/10.1016/j.geomorph.2019.106990

Shahabi, H., Khezri, S., Ahmad, B. Bin, Hashim, M., 2014. Landslide susceptibility mapping at central Zab basin, Iran: A comparison between analytical hierarchy process, frequency ratio and logistic regression models. Catena 115, 55-70. https://doi.org/10.1016/j.catena.2013.11.014

Shao, X., Xu, C., Ma, S., Zhou, Q., 2019. Effects of Seismogenic Faults on the Predictive Mapping of Probability to Earthquake-Triggered Landslides. ISPRS Int. J. Geo-Information 8, 328. https://doi.org/10.3390/ijgi8080328

Sperrevik, S., Gillespie, P.A., Fisher, Q.J., Halvorsen, T., Knipe, R.J., 2002. Empirical estimation of fault rock properties. Nor. Pet. Soc. Spec. Publ. 11, 109-125. https://doi.org/10.1016/S0928-8937(02)80010-8

Stucchi, M., Meletti, C., Montaldo, V., Akinci, A., Faccioli, E., Gasperini, P., Malagnini, L., Valensise, G., 2004. Pericolosità sismica di riferimento per il territorio nazionale MPS04. https://doi.org/10.13127/sh/mps04/ag

Tripathi, S., Bhardwaj, A., Poovammal, E., 2018. Approaches to Clustering in Customer Segmentation. Int. J. Eng. Technol. 7, 802-807. https://doi.org/10.14419/ijet.v7i3.12.16505

Valensise, G., Vannoli, P., Burrato, P., Fracassi, U., 2020. From Historical Seismology to seismogenic source models, 20 years on: Excerpts from the Italian experience. Tectonophysics 774, 228189. https://doi.org/10.1016/j.tecto.2019.228189

van Westen, C.J., van Asch, T.W.J., Soeters, R., 2006. Landslide hazard and risk zonation - Why is it still so difficult? Bull. Eng. Geol. Environ. 65, 167-184. https://doi.org/10.1007/s10064-005-0023-0

Vannoli, P., Burrato, P., Fracassi, U., Valensise, G., 2012. A fresh look at the seismotectonics of the Abruzzi (Central Apennines) following the 6 April 2009 L'Aquila earthquake (Mw 6.3). Ital. J. Geosci. 131, 309-329. https://doi.org/10.3301/IJG.2012.03

Varnes, D., 1984. Landslide hazard zonation : A review of principles and practice, Natural Hazards. UNESCO, Paris, France.

Vezzani, L., Ghisetti, F., 1998. Carta geologica dell'Abruzzo - Scala 1:100.000. S.E.L.C.A., Firenze, Italy.

Villani, F., Civico, R., Pucci, S., Pizzimenti, L., Nappi, R., De Martini, P.M., Agosta, F., Alessio, G., Alfonsi, L., Amanti, M., Amoroso, S., Aringoli, D., Auciello, E., Azzaro, R., Baize, S., Bello, S., Benedetti, L., Bertagnini, A., Binda, G., Bisson, M., Blumetti, A.M., Bonadeo, L., Boncio, P., Bornemann, P., Branca, S., Braun, T., Brozzetti, F., Brunori, C.A., Burrato, P., Caciagli, M.,

Campobasso, C., Carafa, M., Cinti, F.R., Cirillo, D., Comerci, V., Cucci, L., De Ritis, R., Deiana, G., Del Carlo, P., Del Rio, L., Delorme, A., Di Manna, P., Di Naccio, D., Falconi, L., Falcucci, E., Farabollini, P., Faure Walker, J.P., Ferrarini, F., Ferrario, M.F., Ferry, M., Feuillet, N., Fleury, J., Fracassi, U., Frigerio, C., Galluzzo, F., Gambillara, R., Gaudiosi, G., Goodall, H., Gori, S., Gregory, L.C., Guerrieri, L., Hailemikael, S., Hollingsworth, J., Iezzi, F., Invernizzi, C., Jablonská, D., Jacques, E., Jomard, H., Kastelic, V., Klinger, Y., Lavecchia, G., Leclerc, F., Liberi, F., Lisi, A., Livio, F., Sardo, L., Malet, J.P., Mariucci, M.T., Materazzi, M., Maubant, L., Mazzarini, F., McCaffrey, K.J.W., Michetti, A.M., Mildon, Z.K., Montone, P., Moro, M., Nave, R., Odin, M., Pace, B., Paggi, S., Pagliuca, N., Pambianchi, G., Pantosti, D., Patera, A., Pérouse, E., Pezzo, G., Piccardi, L., Pierantoni, P.P., Pignone, M., Pinzi, S., Pistolesi, E., Point, J., Pousse, L., Pozzi, A., Proposito, M., Puglisi, C., Puliti, I., Ricci, T., Ripamonti, L., Rizza, M., Roberts, G.P., Roncoroni, M., Sapia, V., Saroli, M., Sciarra, A., Scotti, O., Skupinski, G., Smedile, A., Soquet, A., Tarabusi, G., Tarquini, S., Terrana, S., Tesson, J., Tondi, E., Valentini, A., Vallone, R., Van Der Woerd, J., Vannoli, P., Venuti, A., Vittori, E., Volatili, T., Wedmore, L.N.J., Wilkinson, M., Zambrano, M., 2018. A database of the coseismic effects following the 30 October 2016 Norcia earthquake in Central Italy. Sci. Data 5, 180049. https://doi.org/10.1038/sdata.2018.49

Wei, C.L., Rowe, G.T., Haedrich, R.L., Boland, G.S., 2012. Long-Term Observations of Epibenthic Fish Zonation in the Deep Northern Gulf of Mexico. PLoS One 7. https://doi.org/10.1371/journal.pone.0046707

Xu, C., 2015. Preparation of earthquake-triggered landslide inventory maps using remote sensing and GIS technologies: Principles and case studies. Geosci. Front. 6, 825–836. https://doi.org/10.1016/j.gsf.2014.03.004

960 Xu, C., Xu, X., 2014. Statistical analysis of landslides caused by the Mw 6.9 Yushu, China,
961 earthquake of April 14, 2010. Nat. Hazards 72, 871-893. https://doi.org/10.1007/s11069-014-
962 1038-2

963 Yalcin, A., Reis, S., Aydinoglu, A.C., Yomralioglu, T., 2011. A GIS-based comparative study of
964 frequency ratio, analytical hierarchy process, bivariate statistics and logistics regression methods
965 for landslide susceptibility mapping in Trabzon, NE Turkey. Catena 85, 274-287.
966 https://doi.org/10.1016/j.catena.2011.01.014

967 Yang, W., Qi, W., Wang, M., Zhang, J., Zhang, Y., 2017. Spatial and temporal analyses of post-
968 seismic landslide changes near the epicentre of the Wenchuan earthquake. Geomorphology 276,
969 8-15. https://doi.org/10.1016/j.geomorph.2016.10.010

970 Zhang, S., Zhang, L., Lacasse, S., Nadim, F., 2016. Evolution of Mass Movements near Epicentre of
971 Wenchuan Earthquake, the First Eight Years. Sci. Rep. 6, 36154.
972 https://doi.org/10.1038/srep36154